Shocks in the Solar Wind Between 1 and 8.5 AU: Voyager 1 Observations

Paul R. Gazis

Center for Space Research, Massachusetts Institute of Technology, Cambridge MA 02139

Short Title: Solar Wind Shocks Between 1 and 8.5 AU

Abstract

A survey was made of all interplanetary shocks detected by the plasma science experiment aboard the Voyager 1 spacecraft between 1.2 and 8.5 AU. Shock normals and shock velocities are determined. The variation of shock frequency and various shock parameters with heliocentric distance is discussed. The following results are observed: 1) Beyond 1.2 AU, the vast majority of shocks were associated with interaction regions between high and low speed streams; of 95 events, only 1 was clearly associated with a transient event. 2) Forward shocks were more numerous and seemed to form closer to the sun than reverse shocks. 3) Forward shocks were stronger than reverse shocks.

The energy balance of three shocks is examined. A close agreement is found between the measured and the predicted pressure ratios across these shocks. The contribution of shocks to the global energy balance is discussed. Shocks are found to have a significant effect in heating the solar wind. However the effect of heating due to shocks appears to be inadequate to explain the heat flux in the solar wind between 1 and 9 AU.

Introduction

An understanding of the origin, evolution, and eventual fate of shocks in the outer heliosphere is important if one is to understand the dynamics and energetics of the solar wind beyond 1 AU.

Observations of interplanetary shocks near 1 AU have been reported by numerous observers over the past two decades [Sonnet et al, 1964; Dryer et al, 1972, 1975; Bavassano et al, 1973; Hundhausen et al, 1970; Chao and Lepping, 1974]. More recently observations at larger heliocentric distances have been reported using data from Pioneer 10 and 11 [Smith and Wolfe: 1976, Smith and Wolfe; 1977; Mihalov and Wolfe, 1979].

Shocks in the solar wind can originate from flares and other solar transients, or they can be caused by the interaction between high and low speed streams of the solar wind. Most shocks in the inner heliosphere ($R < 1$ AU) can be associated with transient events [Chao and Lepping, 1974]. Extensive theoretical and experimental work has been done on the modeling of flare-generated shocks [Hundhausen and Gentry, 1969; Steinolfsen et al, 1975; Borrini et al, 1982].

Beyond 1 AU, the principle source of shocks appears to be stream interactions [Smith and Wolfe, 1979]. This effect was predicted by Sarabai [1963], Parker [1963], Colburn and Sonnet [1966], and others. The name 'interaction region' was coined for the plasma affected by these stream interactions by Smith and Wolfe [1976]. These regions have since come to be called 'co-rotating interaction regions' (CIR's) since the stream structure persists for several rotation periods and the entire quasi-stationary structure rotates with the solar rotation period. The configuration of low

speed stream, forward shock, shocked plasma, reverse shock, and high speed stream is diagrammed in Figure 1.

Numerical models for the formation and evolution of CIR's have been constructed using a two-dimensional MHD approximation [Hundhausen, 1973a, 1973b; Dryer et al, 1978; Steinolfsen and Dryer, 1978]. A comparison between theory and observation has beeen made for the limited periods during multiple spacecraft line-ups [Burlaga et al, 1983]. More recently, models have been devised using a full set of three-dimensional MHD equations [Pizzo, 1983]. However no attempt has been made to compare model predictions concerning shock evolution with observations of a large (>12) sample of shocks. Furthurmore, none of these models treat shocks explicitly as such. Instead, finite dissipative terms are introduced the handle regions containing a large jump in plasma parameters.

In order to draw reliable conclusions concerning the evolution of shocks in the outer heliosphere, one must conduct a survey of a large number of shocks. To learn the average contribution of shocks to heating of the solar wind, one must have a sufficiently large quantity of shock data that the averages are statistically meaningful. Finally, a new study of interplanetary shocks between 1 and 10 AU using Voyager spacecraft data should provide a useful comparison with Pioneer observations in this regions because the Voyager and Pioneer spacecraft traversed this region in very different portions of the solar cycle.

The Voyager 1 spacecraft was launched in late 1977. A plot of the Voyager spacecraft trajectories together with the orbits of Earth, Jupiter and Saturn is shown in Figure 2. Between day 300 of 1977 and day 262 of 1980, the spacecraft traversed the region between 1.2 and 8.5 AU from the sun. During

this time, a large number of shock events in the solar wind were observed by the plasma science experiment aboard the spacecraft. Due to the irregular nature of the solar wind stream structure during the rising portion of the solar cycle when these observations were made, it is sometimes difficult to determine which features are transient events and which are co-rotating, especially if flares arise from longitudes near to the source regions of high speed streams. Nevertheless, only one of the shocks that were observed was associated with a stream feature that did not recur for at least three solar rotations: the shock of day 260 of 1979.

Background

Co-rotating shocks are formed by the interaction of high and low speed streams in the solar wind. In principle, four shocks could form as a result of the interaction. Two would be fast and slow forward shocks, propagating downstream into the low speed stream, and two would be fast and slow 'reverse' shocks, which are convected downstream while propagating upstream into the high speed stream. Usually the two slow shocks are not observed. Between the forward and reverse shocks a region of shocked gas of intermediate velocity and enhanced density and temperature forms. In the Voyager 1 data, stream-produced shocks appear only beyond a heliocentric distance of 2-3 AU. Thereafter stream-produced shocks appear frequently with one or more shocks appearing per solar rotation.

At a shock, the MHD equations become the Rankine-Hugoniot relations describing the jumps in the plasma and the magnetic field parameters. If the bracket operator, [], represents the difference between the post- and

pre-shock values, the subscripts n and t represent the components normal to and parallel to the shock, and $\vec{U}$ is bulk velocity in the shock rest frame, the relations become:

$$[\rho U_n] = 0 \qquad \text{mass flux} \qquad (1)$$

$$[\rho U_n U_t - B_n B_t/4\pi] = 0 \qquad \text{tangential shear balance} \qquad (2)$$

$$[\rho U_n^2 + p + B_t^2/8\pi] = 0 \qquad \text{normal pressure balance} \qquad (3)$$

$$[B_n] = 0 \qquad \text{normal B-field continuity} \qquad (4)$$

$$[U_n B_t - U_t B_n] = 0 \qquad \text{tangential E-field continuity} \qquad (5)$$

where ρ is the mass density (gm cm^{-2}), and p is the isotropic pressure.

Assuming a polytrope approximation, one can write an energy conservation equation:

$$\left[\frac{1}{2}(U_t^2+U_n^2) + \frac{\gamma}{\gamma-1}\frac{p}{\rho} + \frac{1}{4\pi\rho}B_t^2 + \frac{B_t B_n U_n}{4\pi\rho U_n}\right] = 0 \qquad (6)$$

However there is no reason to assume that the polytrope approximation is valid in the region of a shock.

From equations 1), 2), and 4), one can obtain:

$$[B_t(f_m U_n - B_n^2/4\pi)] = 0 \quad \text{where the normal mass flux } f_m = \rho U_n \qquad (7)$$

One can then define three possible cases:

Case 1: $f_m U_{1n} - B_n^2/4\pi > 0$ Fast Shock

In the case of a fast shock, the Alfven mach number of the shock is greater than one. Since f_m and B_n are continuous, the jump in density across the shock has the same sign as the jump in the B-field magnitude.

Case 2: $f_m U_{1n} - B_n^2/4\pi < 0$ Slow Shock

In the case of a slow shock, the Alfven mach number is less than one, and the jump in density across the shock has the opposite sign from the jump in B-field magnitude. Since the shock speed is less than the Alfven speed, a slow shock could in principle decay into a pressure wave.

Case 3a: $f_m U_{1n} - B_n^2/4\pi = 0$ Rotational Discontinuity

A rotational discontinuity, or 'Alfven shock' is essentially a finite amplitude Alfven wave. The plasma bulk velocity does not vary across the discontinuity and the discontinuity propagates at the Alfven speed relative to the unshocked plasma.

Case 3b: $U_n = 0$ Tangential Discontinuity

Tangential discontinuities do not propagate in the plasma. Tangential discontinuities frequently occur at stream interfaces [Gosling et al. 1978].

Unlike shocks, neither rotational nor tangential discontinuities transform bulk kinetic energy into thermal energy. Thus, neither form of discontinuity affects the energy balance. Neither discontinuities nor their consequences are studied in this paper.

The Method of Locating Shocks

An attempt was made to locate all of the shocks observed by the Voyager 1 spacecraft. No similar attempt has yet been made to study the Voyager 2 data due to the fact that the Voyager 2 data are noisier and have many data gaps. Several competing methods were used to search the Voyager 1 plasma data for shocks.

In the initial search, 27-day plots were made of hourly averages of the Voyager 1 plasma data from Day 260 1977 to Day 300 1980. The density and temperature profiles were visually examined for correlated jumps in density and temperature. Approximately 70-80% of the shocks observed were detected by this visual search. The remaining 20-30% of the shocks were too small to be stand out prominently.

In the second search, a computer algorithm was written to list all velocity jumps of greater than 20 km-sec^{-1} in the Voyager 1 hourly averages which had correlated or anti-correlated density jumps. Approximately 98% of the shocks were detected by the computer search, but it picked up 2-3 spurious events for every real shock. These spurious events were due to data gaps, slow variations of solar wind parameters which appeared discontinuous in the hourly averaged data, or fluctuations in velocity which proved not to be

correlated with jumps in density and temperature when the high resolution data were examined. These causes were all of roughly equal importance.

These two lists were then compared with plots of the highest resolution plasma data from Voyager 1. Table 1 shows a final list of those events which might be candidates for shocks. Events which involved a discontinuous jump in the plasma data were listed as 'shocks'. Events which involved changes in the plasma data which resembled shocks but had a finite width of several minutes were listed as 'slopes'. Data gaps across which changes in plasma bulk velocity, density, and temperature occured which were consistent with the occurrence of a shock were called 'gaps'. The lengths of these gaps are indicated in Table 1.

An independant search was made of three months of the plots of the high resolution plasma data between 3 and 4 AU to determine how many shocks might have been missed by the search of the hourly average data. No new shocks were located.

Due to the presence of waves and random fluctuations, it is difficult to search for shocks with small velocity jumps. Slow variations of solar wind parameters frequently cause small apparently discontinuous jumps in the hourly averaged data. For this reason, the hourly averaged data were only searched for velocity jumps of greater than 20 km-sec^{-1}. Many of the shocks located by these searches proved to have velocity jumps of less than 20 km-sec^{-1} when the high resolution data were examined. But these surveys still have a lower detection threshold of approximately 20 km-sec^{-1} in velocity jump.

Figure 3 shows a histogram of the shock velocity jumps. This histogram is strongly peaked near the detection threshold. It is unclear whether this peak is due to a real absence of shocks with velocity jumps of less than 20

km-sec^{-1}, or whether it is due to selection effects. However a more recent search of a limited period of Voyager 2 spacecraft data suggests that there are a large number of shocks lying below this detection limit.

The Method of Determining Shock Normals

A large number of techniques have been proposed for determining shock normals [Colburn and Sonnet, 1966; Lepping and Argentiaro, 1971]. The method used here utilizes both plasma and magnetic data, but in the interest of speed it does not attempt a least squares fit to all of the Rankine-Hugoniot relations.

From Equations 4 and 5, one can obtain the 'coplanarity theorem' [Colburn and Sonett, 1966] which states that the shock normal must be aligned with:

$$(\vec{B}_1 \times \vec{B}_2) \times (\vec{B}_2 - \vec{B}_1) \tag{8}$$

where the subscripts 1 and 2 refer to the values of the unshocked and the shocked parameters respectively.

There are several practical problems in the use of this expression: The pre- and post-shock magnetic field are often nearly parallel, particularly for qusai-perpendicular shocks (shocks with normals approximately perpendicular to the B-field in the unshocked plasma). Because of fluctuations in the post shock magnetic field, it is sometimes difficult to determine with precision. These problems can be mitigated by utilizing the velocity data: From the mass flux equation and the continuity of the normal B-field one can obtain an alternate form of the co-planarity theorem [Abraham-Schrauner and Yun, 1976]:

$$\hat{n} \parallel (\Delta\vec{V}-(\Delta\vec{V}\cdot\Delta\vec{b})\Delta\vec{b}) \qquad \text{where } \Delta\vec{b} = (\vec{B}_2-\vec{B}_1)/\|\vec{B}_2-\vec{B}_1\| \text{ is a unit vector} \qquad (9)$$

The uncertainty in this expression is generally much smaller than that in Equation 8 except for the case of quasi-parallel shocks.

If the magnetic field is small so that the dynamic pressure is very much greater than the dynamic pressure ($M_A>>1$, such as is the case for fast shocks), then a third expression for the shock normal can be derived from Equation 1. One can obtain the following expression for the shock velocity [Lepping and Argentiero, 1971]:

$$\vec{V}_s = [\hat{n}\cdot(\rho_2\vec{V}_2-\rho_1\vec{V}_1)/(\rho_2-\rho_1)]\hat{n} \qquad (10)$$

If one neglects the magnetic pressure in the Rankine-Hugoniot relations, the tangential shear balance equation becomes:

$$[\rho U_n U_t] \cong 0 \qquad (11)$$

But (11) and (1) together imply that $[V_t] \cong 0$ across the shock, or:

$$\vec{V}_s \cong \frac{(\rho_2\vec{V}_2-\rho_1\vec{V}_1)}{\rho_2-\rho_1} \qquad (12)$$

Equation 12 is rigorously true if B=0.

The error due to neglecting the contribution of the magnetic shear to the tangential shear balance equation is of the order of the ratio of the two terms in Equation 2, or:

$$\frac{\delta U_t}{U_n} \approx \frac{B_n B_t}{4\pi\rho U_n^2} \qquad (13)$$

For fast shocks, the shock normal is calculated using (12) and compared with the normal obtained from the alternate co-planarity relation (9). If the two normals agree, the normal determination is considered to be accurate. For slow shocks the shock normals and velocities are determined using only Equation 9.

A typical event, the forward shock seen at 0455 day 313 1979, is shown in Figure 4. The various shock parameters are measured for the data point immediately preceeding and immediately following the shock. If significant oscilations exist in some parameter, the peak values of the oscillation closest to the shock are measured. The mean value and half of the peak-to-peak value of that oscillation are taken to be the mean value and the uncertainty respectively of that parameter. Other methods for the estimation of shock parameters are possible, this particular method was chosen for reasons of convenience.

Typical fluctuations in the radial velocity are on the order of 1%. The fluctuations in the other parameters are larger, usually of order 10% and sometimes as large as 30%. For quasiperpendicular shocks, this implies an angular uncertainty in the shock normal determination of approximately 15° and an uncertainty of at least 10 km-sec^{-1} in the velocity determination.

Quality of the Determinations of Shock Normals

Two techniques are used to evaluate the quality of the shock normal

determination. The first, mentioned in the preceeding section, is to compare the direction of the shock normal determined through use of the continuity equation with the direction of the shock normal determined using the coplanarity theorem. This technique is applicable only for fast shocks.

Figure 5 shows a histogram of the angle between the normals determined for each fast shock by the two methods. The largest source of disagreement is due to the error in neglecting the effect of the magnetic pressure when using only the continuity equation to determine the shock normal. This error is expressed in Equation 13. If M_{An} is of the order 3, then $\delta\theta$ is typically of order $\pm 20^{\circ}$. For 64 of the 71 fast shocks observed, the disagreement between the two normal determinations was of this order. The remaining 7 cases were examined in detail. In each case, the disagreement was attributable to unusually large uncertainties in the measurements of the basic shock parameters.

From the mass flux equation, the tangential E-field continuity equation, and the tangential shear balance equation, one can obtain:

$$\frac{N_1}{N_2} = \frac{B_{1t}}{B_{2t}}\left[1+\left(\frac{B_{2t}}{B_{1t}} -1\right)M_{An}^{-2}\right] \qquad (14)$$

where the perpendicular Alfven Mach number $M_{An} = U_{1n}\left(B_{1n}^2/4\pi\rho_1\right)^{-1/2}$.

The uncertainty in (14) can be written:

$$\delta\left(\frac{N_1}{N_2}\right) = \frac{\delta B_{1t}}{B_{1t}}\left[\frac{N_1}{N_2} - \frac{B_{2t}}{B_{1t}}M_{An}^{-2}\right] - \frac{\delta B_{2t}}{B_{2t}}\left[\frac{N_1}{N_2} + \frac{B_{2t}}{B_{1t}}M_{An}^{-2}\right]\Big] -2\,\frac{\delta M_{An}}{M_{An}}\left(\frac{B_{2t}}{B_{1t}} -1\right)M_{An}^{-2}\Big] \qquad (15)$$

If there are fluctuations of 10% in the measured densities and B-fields, it is possible for the predicted and measured density ratios to disagree by a

factor of 1.7. For a shock with a large Alfvenic Mach number, $M_{An} > (B_{2t}/B_{1t}-1)^2$, the uncertainty in the perpendicular Mach number can be an even larger source of error: As the angle Θ between the shock normal and the B-field approaches 90°, small uncertainties in Θ can lead to large uncertainties in the predicted density ratio.

Figure 6 shows a histogram of the theoretical density ratio divided by the density ratio measured for each shock. The normal direction was determined using the form of the co-planarity relation in Equation 9. For 69 of the 82 events, the agreement of the two density ratios is within a factor of two. As shown below, this is as good as can be expected given the uncertainties in the measured data.

For all of the events observed at Voyager 1, the error in the determination of the shock normal inferred from the error in the predicted density ratio is within the uncertainty in the shock normal set by the uncertainty in the measurement of the data. For 69 of these 82 events, the determinations of the shock normals are accurate to within at least 15°.

Shocks in the Solar Wind: Observations

Figures 7 through 10 [Gazis and Lazarus, 1983] show the variation of various shock parameters with heliocentric distance.

Figure 7 shows a plot of the frequency of occurence of forward shocks and reverse shocks versus heliocentric distance. The frequency of occurence of shocks was determined by taking a running average of the time spacing between shocks for groups of twelve shocks with a slip of one shock between successive averages. The first two shocks in Table 1 were not included in these plots

since they are imediately followed by the Voyager 1 data gap between day 320 1977 and day 100 1978.

As can be seen, there is a distinct difference between the radial profiles of the frequency of occurence of forward shocks and reverse shocks. The forward shocks originate earlier in the solar wind, occur more frequently, and continue to be observed out to greater distances than the reverse shocks. The fact that the observed shock frequency decreases with increasing heliocentric distance does not necessarily mean that some of the shocks actually disappear as they propagate outwards from the sun. The shocks might continue to exist but drop below our detection threshold of $\Delta V=20$ km-sec^{-1}. It also probable that the apparent radial variation of shock frequency is in fact a temporal variation. In view of the lack of any obvious change in the stream structure seen by IMP 8 at 1 AU, and the lack of any change in the average of the bulk parameters seen at 1 AU, this source seems unlikely, but until a complete list is made of all shocks observed by the Voyager 2 spacecraft, it will be difficult to separate radial and temporal variations.

Superimposed upon the radial variation of shock frequency are large temporal variations, particularly for the forward shocks in late 1978 when the Voyager 1 spacecraft was near 5.5 AU. These temporal variations do not correspond to any obvious variation in the average plasma bulk parameters observed at the IMP 8 spacecraft during the corresponding time. (It is interesting to note, though, that the large drop in frequency of forward shocks observed at 5.5 AU occurs in mid-late 1979, at the onset of a sudden decrease in geomagnetic storm activity).

It is instructive to plot the radial variation of various parameters related to the strength of shocks:

Figure 8 shows a plot of the running average of the speeds of twelve successive shocks (forward shocks and reverse shocks) plotted versus heliocentric distance. Twelve-shock averages were chosen as the best compromise between poor time resolution and excessive fluctuations in the average. As with shock frequency, the shock speeds for forward shocks are uniformly higher than the shock speeds for reverse shocks.

Figure 9 shows a plot of a twelve-shock running average of the shock velocity jump for forward shocks and reverse shocks. Since the shock velocity jump is related to shock speed, it is no surprise that the velocity jumps across forward shocks are higher and change more slowly with heliocentric distance than do the velocity jumps across reverse shocks. The average of the velocity jump across the reverse shocks declines approximately twice as fast as the average of the velocity jump across the forward shocks.

Figure 10 shows a plot of twelve-shock running averages of the density ratios across the shock for forward shocks and reverse shocks versus heliocentric distance. Unlike the shock frequency, speed, and velocity jump, the density ratio across both the forward and the reverse shocks remains fairly constant with increasing heliocentric distance. The twelve-shock average of the density ratios across the forward shocks is between 1.6 and 2.8, though individual shocks have density ratios which range from ≥ 1 to 4. The reverse shocks are somewhat weaker with an average density ratio of approximately 2, but the range of density ratios for individual reverse shocks is much the same as for forward shocks.

A Model of Shock Evolution

For a perpendicular fast shock with a radial normal, the shock speed is determined only by the continuity equation. The equation for shock speed, V_s, in the spacecraft frame is (12). For purely radial velocities, this can be rewritten:

$$V_s = \frac{xV_2 - V_1}{x-1} \quad \text{where the density ratio } x = \frac{\rho_2}{\rho_1} \tag{16}$$

The geometry of forward and reverse shocks as seen in the spacecraft frame is shown in Figure 11. For the forward shock, $\rho_2 > \rho_1$ and $V_s > V_2 > V_1$. For the reverse shock, $\rho_2 > \rho_1$ and $V_1 > V_2 > V_s$.

Taking the convective derivative, (16) becomes:

$$\frac{D}{Dt}V_s = \frac{1}{x-1}\left(\frac{V_2(x-1)-(xV_2-V_1)}{x-1}\frac{D}{Dt}x + x\frac{D}{Dt}V_2 - \frac{D}{Dt}V_1\right) \tag{17}$$

The density ratio, x, and the post shock velocity, V_2, vary only slowly with respect to R and can be treated as constant as the shocks propagate outwards from the sun. Therefore, for typical values of shock parameters such as in Table 2, the first two terms on the right side of (17) are negligable and one can write:

$$\frac{D}{Dt}V_s = -\frac{1}{x-1}\frac{D}{Dt}V_1 \tag{18}$$

The pre-shock velocity V_1 changes due to the fact that the shock is propagating into a velocity gradient. If one takes the convective derivative of V_1 in the shock frame, one obtains:

$$\frac{D}{Dt}V_1 = \frac{\partial}{\partial t}V_1 + V_s \frac{\partial}{\partial R}V_1 \tag{19}$$

(But the convective derivative in the spacecraft frame vanishes, or:)

$$\frac{D}{Dt}V_1 = \frac{\partial}{\partial t}V_1 + V_1 \frac{\partial}{\partial R}V_1 = 0 \tag{20}$$

Using (20) to eliminate the partial time derivative, (19) becomes:

$$\frac{D}{Dt}V_1 = (V_s - V_1)\frac{\partial}{\partial R}V_1 = U_1\frac{\partial}{\partial R}V_1 \tag{21}$$

And (18) becomes:

$$\frac{D}{Dt}V_s = - \frac{1}{x-1} U_1 \frac{\partial}{\partial R}V_1 \tag{22}$$

or:

$$\frac{D}{Dt}U_1 = - \frac{x}{x-1} U_1 \frac{\partial}{\partial R}V_1 \tag{23}$$

If the shock decays when the upstream flow velocity in the shock frame drops below the Alfven speed, then the lifetime of a fast shock will be approximately:

$$\tau_L \cong (U_1 - V_A)\left(\frac{D}{Dt}U_1\right)^{-1} \tag{24}$$

Alternatively since $U_1 = (x/x-1)\Delta V$, if the shock drops below the detection threshold when the velocity jump, ΔV, drops below some value, ΔV_t, then the shock will have an apparent lifetime:

$$\tau_L \cong (U_1 - \frac{x}{x-1}\Delta V_t)(\frac{D}{Dt}U_1)^{-1} \qquad (25)$$

So in the case of a perpendicular fast shock, a shock which initially has a larger shock speed will survive longer than a shock which starts with a low shock speed. In the case of shocks having the same shock speed a forward shock, since it is convected outwards from the sun at a higher velocity than a reverse shock, will propagate out to a larger heliocentric distance before it disappears.

Typical numbers for interplanetary shocks at 4AU are shown in Table 2. There is reasonable agreement with the radial profiles observed in Figure 9.

A Model of Shock Formation

If one takes the values of the plasma parameters before and after the interaction region and attempts to use the six Rankine-Hugoniot relations, (1)-(6), to determine a set of shock velocities and the density ratios which will reproduce these values, one has 12 equations in 14 unknowns: $\vec{V}_f$ and $\vec{V}_r$ of the forward and reverse shocks, and $\vec{V}$, ρ, p, $\vec{B}$ of the plasma inside the interaction region. Hence there is no intrinsic reason why either the forward or the reverse shock should be stronger. The reason for the observed asymmetry must lie in the manner in which the shocks form.

If one assumes that the formation of an infinite radial gradient in density is a sufficient condition for the formation of a shock, then one can attempt to estimate the heliocentric distance at which shocks will form.

Figure 12a shows a stream seen by Voyager 1 between day 288 and day 300

of 1977 when Voyager 1 was at 1.2 AU. In this stream the density is aproximately anti-correlated with the bulk velocity. This rough anti-correlation of density and bulk velocity, in which the mass flux stays almost constant with respect to time, is typical of the flow near 1 AU. The velocity minimum and density maximum are located on day 291, and the velocity maximum and density minimum are located on day 294. The region between days 291 and 294 will later become the 'interaction region'. In this region, the solar wind plasma is being compressed by the negative radial velocity gradient.

Note that the velocity profile of this stream is not completely anti-symmetric about the midpoint of the interaction, on day 292. The velocity gradient in the high speed stream, after the passage of the interaction region, is less than the velocity gradient in the low speed stream. This structure is typical [Gosling et al., 1976]. As a consequence, the solar wind number density in the low speed stream will decrease with heliocentric distance more rapidly than will the number density of the high speed stream.

The structure of a typical stream at 1.7 AU, still prior to the onset of stream-generated shocks, is shown in Figure 12b. The velocity profile retains roughly the same structure as the velocity profile at 1.2 AU, though the region of negative velocity gradient is narrower. The velocity minimum is on day 347 and the velocity maximum is on day 349. However, compression within the interaction region has radically changed the structure of the density profile. The density now has a maximum on day 348, near the center of the interaction region. Also, as mentioned in the discussion of the stream at 1.2 AU, the differing velocity gradients in those portions of the high and low speed streams which border the interaction region have led to different rates

of change of the density, so that the densities of the high and low speed streams are now roughly equal.

It has been assumed that the question of whether the forward or the reverse shock forms first will be determined by which radial density gradient steepens faster; the radial density gradient in the region in which the forward shock is to form, or the radial density gradient in the region in which the reverse shock is to form. But it is possible to calculate the rate of change of the radial density gradients which bound the interaction region. The gradients of thermal and magnetic pressures are still much less than the gradient of the dynamic pressure, so the only important MHD equation is the continuity equation. Considering only the radial derivatives, this becomes the one-dimensional continuity equation:

$$\frac{D}{Dt}(NR^2) = -NR^2 \frac{\partial V}{\partial R} \tag{26}$$

The rate of change X of the radial gradient of NR^2 is then approximately:

$$X = \frac{D}{Dt} \frac{\partial(NR^2)}{\partial R} = - \frac{\partial(NR^2)}{\partial R} \frac{\partial V}{\partial R} - (NR^2)\frac{\partial^2 V}{\partial R^2} \tag{27}$$

If one the stream in Figure 12B is typical of the streams at 1.8 AU, and that the stream pattern is being convected outwards at 400 km-sec^{-1}, then the average plasma parameters for a compression region at 1.8 AU are shown in Table 3.

At 1.8 AU the density gradient in the region that will become the forward shock is already steeper than the density gradient in the region that will become the reverse shock, and is steepening faster, which suggests that the forward shock will form first. Note that the forward shock is expected to

form first only because of the particular initial conditions observed in this data. Obviously it is possible to construct velocity and density profiles which lead to an early formation of reverse shocks. A more exact determination of the location of the onset of forward and reverse shocks would require a detailed numerical model of solar wind stream evolution. Models of this sort have been constructed by Hundhausen [1973a] and Pizzo [1982], but are beyond the scope of this paper.

Evolution and Structure

Siscoe [1976] predicted that on the average shock surfaces would conform to the Parker spiral. Figure 13 shows a plot of the azimuthal angle of the shock normals versus heliocentric distance. The value expected for shock surfaces which conform to the Parker spiral is shown in the curved trace. The apparent temporal variation in shock azimuthal angle is too large to allow a ready determination of the variation of the average azimuthal angle with heliocentric distance. However Parker spiral angle falls within the range of observed azimuthal angles.

Figure 14 shows a plot of the north-south shock angles versus heliocentric distance. The average north-south angle remains fairly constant at zero. The variations about this mean are of the order of ten degrees.

The large deviations of the shock azimuthal and north-south angles from the expected directions could be taken to mean that the shock surface is not smooth but contains large scale ripples. Alternatively, it is possible that the boundaries of the co-rotating interaction regions are not one continuous shock surface but consist of a large number of smaller intersecting shock

surfaces. To accurately reconstruct the large scale structure of co-rotating shocks, it will be necessary to include data from more than one spacecraft.

Shock Energy Balance and Contribution to Global Heating

A detailed study of the energy balance for a shock requires knowledge of the electron temperatures before and after that shock. Electron temperatures for three shocks were provided by Sittler (private communication). The contribution of the alpha particles to the total pressure was ignored. The shocks in question were the shocks of 1507 day 13 1979, 2056 day 17 1979, and 1920 day 176 1979. The pre and post shock parameters for these shocks are listed in Table 4. The electron distribution functions have been divided in to a thermal 'core' distribution, and a non-thermal 'halo' distribution, and the parameters for these two distributions listed separatly.

For the shocks of day 17 and day 176, the agreement between the measured pressure ratio and the predicted pressure ratio is quite good. The measured and the predicted pressure ratio (see below) do not agree quite as well for the shock of day 13, however the uncertainty in the measured pressure ratio for this event is quite large, primarily due to the uncertainty in unshocked electron density.

From Equations 1 and 3, one can obtain an expression for the ratio of thermal energy density across a shock:

$$\frac{p_2}{p_1} = \left[1+r_1\left(1-\frac{N_1}{N_2}\right) + \frac{1}{\beta_1}\left(1-\left(\frac{B_{2t}}{B_{1t}}\right)^2\right)\right] \qquad \text{where} \quad r_1 = \rho_1 U_{1n}^2/N_1 kT_1 \quad \beta_1 = N_1 kT_1/(B_1^2/8\pi) \qquad (28)$$

This relation is used to obtain the predicted pressure ratios shown in Table 4.

For the shocks of day 17 and day 176, the agreement of the measured and the predicted ratio of pre and post shock thermal energy density is well within the uncertainties. For the shock of day 13, the agreement is less good. However, there is a large uncertainty in the observed shock parameters for this shock.

It was not possible to obtain electron data for all of the shocks seen by Voyager 1. However, it is still possible to estimate the magnitude of the heating of the solar wind protons due to shocks:

One can define an average proton heating rate $(\partial E/\partial t)_s$ per shock:

$$(\partial E/\partial t)_s = \langle \Delta e \rangle \langle U_1 \rangle A \tag{29}$$

where $\langle \Delta e \rangle$ is the average jump in proton thermal energy density across a shock and A is the area of the shock surface. Running twelve shock averages of $\langle \Delta e \rangle$ calculated from the proton thermal speed and number density are plotted versus heliocentric distance in Figure 15.

The average number density n_s of shocks is simply the inverse of the product of the area of a shock surface and the radial separation between the shocks or:

$$n_s = \frac{\langle \nu \rangle}{\langle V_s \rangle A} \qquad \text{where } \langle \nu \rangle = \text{average shock frequency} \tag{30}$$

The energy source term h_s due to all shocks will then be the average heating rate per shock times the number density of the shocks, or:

$$h_s \equiv \frac{\langle \nu \rangle \langle \Delta e \rangle \langle U_1 \rangle}{\langle V_s \rangle} \tag{31}$$

Typical values for $\langle v \rangle$, $\langle U_1 \rangle$, and $\langle V_s \rangle$ for forward and reverse shocks, at 4 and 8 AU are shown in Table 5.

The energy source term due to shocks can be fit by a power law:

$$\langle h_s R^2 \rangle = h_0 R^{-\beta} \quad \text{(where R is measured in AU)} \tag{32}$$

$h_0 = 0.38 \times 10^{-14}$ erg-cm^{-3}sec^{-1}, $\beta = 3.3$ for forward shocks

$h_0 = 1.35 \times 10^{-14}$ erg-cm^{-3}sec^{-1}, $\beta = 4.8$ for reverse shocks.

This energy source term is equivalent to the presence of a radial heat flux $\vec{q}_s^{(eff)} = q_s^{(eff)} \hat{e}_R$ where:

$$\frac{\partial}{\partial R}\left(R^2 q_s^{(eff)}\right) = -\langle h_s R^2 \rangle \tag{33}$$

Equation 33 can be solved to give:

$$q_s^{(eff)} R^2 = q_0 R^{-\alpha} \quad \text{where } q_0 = -(1\ \text{AU})\ \frac{h_0}{\alpha} \quad \text{and } \alpha = \beta - 1 \tag{34}$$

$q_0 = 2.47 \times 10^{-2}$ erg-cm^{-2}sec^{-1} $\alpha = 2.3$ for forward shocks

$q_0 = 5.31 \times 10^{-2}$ erg-cm^{-2}sec^{-1} $\alpha = 3.8$ for reverse shocks.

Equation 34 is an expression for the effective energy flux due to heating of the solar wind by stream-produced shocks. This expresssion is not valid at heliocentric distances less than 3 AU since stream-produced shocks do not appear closer to the sun. At 4 AU and 10 AU this effective energy flux is:

	4 AU	10 AU	
forward shocks: $q_s^{(eff)} R^2$ =	1.02×10^{-3}	1.24×10^{-4}	erg cm^{-2} sec^{-1}
reverse shocks: $q_s^{(eff)} R^2$ =	0.27×10^{-3}	0.84×10^{-5}	erg cm^{-2} sec^{-1}

One can compare these quantities with the heat flux necessary to explain the observed radial trends in the solar wind energy fluxes, [Gazis, 1984]:

	1 AU	4 AU	10 AU	
$q_R R^2$ =	2.5×10^{-2}	13.6×10^{-3}	6.9×10^{-3}	erg cm^{-2} sec^{-1}

At 4 and 10 AU, the effective energy flux $q_s^{(eff)}$ due to heating of the solar wind by shocks is an order of magnitude less than the heat flux. The effective energy flux $q_s^{(eff)}$ decreases slightly faster than q_R and by 10 AU, $q_s^{(eff)}$ is a factor of 30 less than q_R.

One source of error in the determination of $q_s^{(eff)}$ is the failure to include shocks with velocity jumps which lie below the detection threshold of 20 km-sec^{-1}. This omission reduces the measured value of $q_s^{(eff)}$. The other major source of error is uncertainty in the determination of the power law exponent β for the variation of h_s with heliocentric distance. This introduces an uncertainty in the magnitude of $q_s^{(eff)}$ of at least a factor of two.

The net result of heating the solar wind protons by interplanetary shocks is the addition of an effective energy flux $q_s^{(eff)}$. This effective energy flux is comparable to or less than the heat flux q_R required to explain the observed radial profiles of proton and electron temperature. As with q_R, $q_s^{(eff)}$ tends to zero as R tends to infinity.

Quasi-Parallel Shocks

A parallel shock should be characterized by a normal parallel to the magnetic field vector and by the fact that the average B-field magnitude does not change across the shock.

There are seven shocks for which the angle between the shock normal and the magnetic field vector is less than 30° and is less than the uncertainty in the normal determination, or for which the B-field magnitude does not vary by more than 10% across the shock. Those shocks considered here to be quasi-parallel are listed in Table 6. There are additional shocks, most notably the shock of 0247 day 296, 1978 which have structure similar to that which might be expected for parallel shocks and have sufficiently high uncertainties in some basic parameters that they might be quasi-parallel shocks. However the uncertainties make these shocks hard to analyze and they have been excluded from the table.

The seven shocks listed in Table 6 have a distinctive structure:

1) Each of these events has significant wave activity upstream and downstream of the shock. In some cases, the wave amplitude is as high as 30% of the shock amplitude. This structure is similar to the structure usually seen upstream of Earth's bow shock in the dawn-to-noon quadrant.

2) Each of these events has a finite thickness, of the order of ten minutes. This corresponds to a spatial thickness of order of 3×10^{5} km.

Slow Shocks

As was discused earlier, slow shocks should be characterised by $M_{An}<1$ and a jump in B-field magnitude of opposite sign to the jump in density. Eleven of the shocks observed at Voyager 1 fulfill these criteria, and they are listed in Table 7.

Both forward and reverse slow shocks are observed, though as for fast shocks, the forward shocks are the more numerous. All of these events are quite weak, with velocity jumps less than 40 km-sec^{-1} and density ratios less than two. The orientations of these shocks are unusual; the shock normals are directed in some cases as much as 90^{o} away from the radial direction.

Finally, the slow shocks show a tendency to occur very close together in time; six of the eleven events observed had some neighboring slow shock occur within eight days. This suggests that some process may exist which generates strings of slow shocks.

Some of these shocks appear to be associated with shock pairs. If so, and if the fast and slow shocks were formed simultaneously, their separation might provide a measure of how long ago these shocks were formed.

Summary and Conclusions

Between late 1977 and late 1980, the principle source of interplanetary shocks observed by the Voyager 1 spacecraft at large heliocentric distances was the interaction of high and low speed streams in the solar wind. These 'stream-produced shocks' begin to appear at a heliocentric distance of between 2 and 3 AU and persist out to the limits of these observations.

Forward shocks appear earlier than reverse shocks in these observations; between 2 to 3 AU as opposed to 4 AU. The forward shocks are also 'stronger' than the reverse shocks: The forward shocks have a higher average speed with respect to the solar wind, a higher average velocity jump, and a higher average density ratio than the reverse shocks.

These stream-produced shocks appear to decay as they propagate outwards from the sun. This decay is consistent with a simple model of shock evolution but it is not clear, from observations from only a single spacecraft, whether this decay represents a true radial variation, whether it is due to temporal effects or whether it is due to selection effects in the shock survey.

It is worth noting that stream-generated shocks can persist even after the streams that generated them have eroded away. Thus, even if the solar wind at large heliocentric distances is dominated by 'pressure waves' rather than streams as has been suggested by Burlaga [1983], one would still expect to observe stream-generated shocks.

The majority (70%) of the quasi-perpendicular shocks are fast shocks. The Alfvenic mach numbers range from 1 to 9 and the density ratios range from 1.5 to 4. There are also 11 cases of perpendicular slow shocks, and 7 cases of quasi-parallel shocks.

For three shocks there are corresponding electron measurements. The measured and the predicted pressure ratios across the shocks agree, implying that there is no need to invoke the acceleration of high energy particles to explain the energy balance of these events. However the uncertainty in the pressure measurements is sufficiently large that as much as 10% of the total energy density as measured in the shock frame could be lost into high energy particles or waves without being noticable.

The effect of stream-produced shocks in heating the solar wind at large heliocentric distances can be expressed by the introduction of an additional heat source into the MHD equations. At 4 AU, the effect of this heat source is comparable to or less than the heat flux required to explain the observed radial variation of the solar wind temperature [Gazis, 1984]. The effect of shock heating appears to decrease more rapidly with heliocentric distance than does the heat flux. However it is not clear how much of this decrease is due to real radial variation, how much is due to temporal variations in the solar wind stream structure, and what the effect is of shocks with velocity jumps to small to be detected by this survey.

I would like to thank E. Sittler for providing electron data. I would like to thank A. J. Lazarus, S. Olbert, J. D. Sullivan, and C. Goodrich for their suggestions, discussions and criticism. This work was supported by the National Aeronautics and Space Administration through the Voyager program, Contract 953733 (JPL).

References

Abraham-Shrauner B. and S. H. Yun, Interplanetary shocks seen by the Ames plasma probe on Pioneer 6 and 7, J. Geophys. Res., 81, 2097, 1976

Bavassano, B., F. Mariani, and N. F. Ness, Pioneer 8 Observations and interpretations sixteen interplanetary shock waves observed in 1968, J. Geophys. Res., 78, 4535, 1973

Borrini, G., J. T. Gosling, S. J. Bame, and W. C. Feldman, An analysis of shock wave disturbances observed at 1 AU from 1971 through 1978, J. Geophys. Res., 81, 4363, 1982

Burlaga, L. F., and J. K. Chao, Reverse and forward slow shocks in the solar wind, J. Geophys. Res., 76, 7516, 1971

Burlaga, L. F. Corotating pressure waves without fast streams in the solar wind, J. Geophys. Res., 88, 6085, 1983

Burlaga, L. F., A. J. Lazarus, R. Schwenn, and H. Rosenbauer, Dynamical evolution of interplanetary magnetic fields and flows between 0.3 and 8.5 AU, Geophys. Res. Lett., 10, 413, 1983.

Chao, J. K., and R. H. Lepping, A correlative study of SSC's, interplanetary shocks, and solar activity. J. Geophys. Res., 79, 1799, 1974

Colburn, D. S., and Sonnet, C. P., Discontinuities in the solar wind, Space Sci. Rev., 5, 439, 1966

Dryer, M., Z. K. Smith, G. Endrad, and J. H. Wolfe, Pioneer 7 observations of the August 29, 1966 interplanetary shock-wave ensemble, Cosmic Electrodynamics, 3, 184, 1972

Dryer, M., Z. K. Smith, T. Unti, J. D. Mihalov, B. F. Smith, J. H. Wolfe, D. S. Colburn, and C. P. Sonett, Pioneer 9 and Ogo 5 observations of the

interplanetary multiple shock ensemble of February 2 1969, J. Geophys. Res., 80, 3225, 1975

Dryer, M., Z. K. Smith, E. J. Smith, J. D. Mihalov, J. H. Wolfe, R. S. Steinolfsen, and S. T. Wu, Dynamic modeling of solar wind co-rotating stream interaction regions observed by Pioneer 10 and 11, J. Geophys. Res., 83, 4347, 1978

Gazis, P. R. and A. J. Lazarus, The radial evolution of the solar wind, 1-10 AU, Solar Wind 5, 509, NASA Conference Publication 2280, ed. M. Neugebayer

Gazis, P. R., Observations of plasma bulk parameters and the energy balance of the solar wind between 1 and 10 AU, J. Geophys. Res.,89, 775, 1984

Gosling, J. T., A. J. Hundhausen, and S. T. Bame, Solar wind stream evolution at large heliocentric distances: experimental demonstration and test of a model, J. Geophys. Res., 81, 2111, 1976

Hundhausen, A. J., and R. A. Gentry, Numerical solutions of flare-generated disturbances in the solar wind, J. Geophys. Res., 74, 2908, 1969

Hundhausen, A. J., S. J. Bame, and M. D. Montgomery, Large scale characteristics of flare associated solar wind disturbances, J. Geophys. Res., 75, 4631, 1970

Hundhausen, A. J., Nonlinear model of high-speed solar wind structure beyond 1 AU, J. Geophys. Res., 78, 1528, 1973a

Hundhausen, A. J., Evolution of large-scale solar wind strutures beyond 1 AU, J. Geophys. Res., 78, 2035, 1973b

Lepping, R. P., and Argentiero, P. D., Single spacecraft method of estimating shock normals, J. Geophys. Res., 76, 4349, 1971

Mihalov, J. D. and J. H. Wolfe, Pioneer 10 studies of interplanetary shocks at large heliocentric distances, Geophys. Res. Lett., 6, 491, 1979

Parker, E. N. Interplanetary Dynamical Processes, p152, Interscience, N. Y. 1963

Pizzo, V., A three dimensional model of corotating streams in the solar wind. 3. Magnetohydrodynamic streams, J. Geophys. Res., 87, 4347, 1982

Rosenau P., and S. T. Suess, Slow shocks in the interplanetary medium, J. Geophys. Res., 82, 3649, 1977

Sarabai, V., Some consequences of non-uniformity of solar wind velocity, J. Geophys. Res., 68, 1555, 1963

Siscoe, G., Three dimensional aspects of interplanetary shock waves, J. Geophys. Res., 81, 6235, 1976

Smith, E. J., and J. H. Wolfe, Observations of interaction regions and co-rotating shocks between one and five AU: Pioneers 10 and 11, Geophys. Res. Lett., 3, 137, 1976

Smith, E. J., and J. H. Wolfe, Observations of evolving solar wind streams and shocks beyond 1 AU, Study of Travelling Interplanetary Phenomena/ 1977, Ed. M. A. Shea, et al., 227, D. Reidal, Hingham, Mass., 1977

Smith, E. J., and Wolfe, J. H., Fields and plasmas in the outer solar system, Space Sci. Rev., 23, 217, 1979

Sonnet, C. P., D. S. Colburn, L. Davis Jr., E. J. Smith, and P. J. Colman Jr., Evidence for a collision-free magnetohydrodynamic shock in interplanetary space, Physs. Rev. Letters, 13, 153, 1964

Steinolfsen, R. S., M. Dryer, and Y. Nakagawa, Interplanetary shock pair disturbances: comparison of theory with space probe data, J. Geophys. Res., 80, 1989, 1975

Steinolfsen, R. S., and M. Dryer, Numerical simulations of MHD shock waves in the solar wind, J. Geophys. Res., 83, 1576, 1978

Figure 1: Schematic representation of the structure of a co-rotating interaction region and its accompanying shocks, as viewed from above the plane of the solar equator.

Figure 2: Spacecraft trajectories for Voyager 1 and 2.

Figure 3: Histogram of the shock velocity jumps.

Figure 4: Time axis plot of various solar wind bulk parameters observed during the shock event of 0455 day 313 1979.

Figure 5: Histogram of the angle between the shock normals calculated from the mass continuity equation alone and the shock normal calculated including the effect of the B-field for the 71 fast shocks.

Figure 6: Histogram of the measured density ratio divided by the density ratio predicted from the tangential pressure equation for all 83 shocks.

Figure 7: Twelve shock running averages of shock frequency plotted versus heliocentric distance for forward shocks and reverse shocks. There is a one shock slip between the successive averages.

Figure 8: Twelve shock running averages of shock speed plotted versus heliocentric distance for forward shocks and reverse shocks. There is a one shock slip between the successive averages.

Figure 9: Twelve shock running averages of shock velocity jump plotted versus heliocentric distance for forward shocks and reverse shocks. There is a one shock slip between the successive averages.

Figure 10: Twelve shock running averages of shock density ratio plotted versus heliocentric distance for forward shocks and reverse shocks. There is a one shock slip between the successive averages.

Figure 11: Schematic representation of plasma parameters in the shock

frame and in the spacecraft frame for a forward shock and for a reverse shock.

Figure 12: Time axis plot of solar wind bulk velocity and density for a stream observed at 1.2 AU and a stream observed at 1.8 AU. The interaction regions are marked.

Figure 13: The individual values of azimuthal angle of the shock normals for all 83 analyzed shocks plotted versus heliocentric distance. The solid trace shows the expected value if the shock surfaces were to conform exactly to the Parker spiral.

Figure 14: The individual values of north-south angle of the shock normals for all 83 analyzed shocks plotted versus heliocentric distance.

Figure 15: Twelve shock running averages of the jump in energy density across each shock plotted versus heliocentric distance all shocks. There is a one shock slip between the successive averages.

Table 1. Voyager 1 Shock Times

Year	Day	Hour	Type	Year	Day	Hour	Type	Year	Day	Hour	Type
1977	301	0655	F	1978	(287-288		F)	1979	42	0557	F
	331	2221	F		289	2205	R		56	0308	R
	347	1215	F		296	.0247	G	Jupiter encounter 59-82			
(1978	33	1650	F		300	1553-1620	R		92	1139	F
	178	2303	F		305	1314	G		93	0716	R
204	2258		F		316	1839-2255	F		112	1140-1924	R
	209	1312	F		321	0828	S		117	1712	R
	213	1440	F		338	0122	G		118	0430	F
	217	0220	S		338	1016-1324	F		128	0520	F
	223	0825	F		341	0946-1343	R		133	0244	F
	228	0614-1537	R		(356-357		F)		133	1057-1812	R
	237	1349-1942	F		360	0432	F		139	2045	F
	241	1543-1944	R	1979	1	0628	G		152	0229	F
	(251	1938	F)		13	1507	F		161	0235	G
	264	0229-1006	F		17	2057	R		(166-167		F)
	267	2142	R		21	1334	G		(174-175		F)
	279	1334	R		29	1850	G		176	1920	F
	284	2130	R		37	2206	F		179	0205	R

F = forward shock

G = forward slope

R = reverse shock

S = reverse slope

unconfirmed events are marked with parenthesis

Table 1. Voyager 1 Shock Times (cont)

Year	Day	Hour	Type	Year	Day	Hour	Type	Year	Day	Hour	Type
1979	191	0946	F	1980	14	0736	R	1980	177	0777	F
	197	1850	F		28	0746	F		178	0631	F
	(206	1630	F)		32	0616	R		201	1511	F
	211	1817-2150	R		34	2246	R		222	1955	F
	217	1120	F		(51	0500	G)		260	2112	S
	220	1714-2132	R		57	0122	R		261	2010	G
	222	0641-1539	R		(60-61		F)		262	0900	G
	226	0531	R		(82-83		F)				
	260-261		R flare		103	0305-0837	R				
	266	0308	R		112	1118	F				
	308	2100	G		117	1447-2008	F				
	313	0455	F		122	1118	F				
	334	0645	G		124	0828-1339	F				
	339	0134	F		146	0439	F				
	346	0403	F		146	0817	F				
	346	1800	G		150	0312	F				
1980	7	0936	F		(152	1320	R)				
	11	0536-1216	R		(159	1203-1900	R)				

F = forward shock

G = forward slope

R = reverse shock

S = reverse slope

Unconfirmed events are marked with parenthesis

TABLE 2. Typical Values and Rates of Change for Shock Parameters

	Forward Shock	Reverse Shock
U_1 =	160 km-sec^{-1}	120 km-sec^{-1}
ρ_2/ρ_1 =	2	2
$\partial V/\partial R$ =	40 km-sec^{-1}AU^{-1}	40 km-sec^{-1}AU^{-1}
V_A =	40 km-sec^{-1}	40 km-sec^{-1}
V_s =	580 km-sec^{-1}	360 km-sec^{-1}
DU_1/Dt =	6.5×10^{-5} km-sec^{-2}	6.4×10^{-5} km-sec^{-2}
DU_1/DR =	16.5 km-sec^{-1}AU^{-1}	26.6 km-sec^{-1}AU^{-1}
τ_L =	23 days	17 days
$\langle V_s \rangle \times \tau_L$ =	7.3 AU	3.0 AU

TABLE 3. Typical Solar Wind Parameters at 1.8 AU, Prior to Shock Formation

	Forward Side	Reverse Side
$\left\langle \frac{\partial}{\partial R}\left(\frac{NR^2}{1\ AU^2}\right)\right\rangle$ =	1.8×10^{2} $cm^{-3}AU^{-1}$	-0.9×10^{2} $cm^{-3}AU^{-1}$
$\left\langle \frac{\partial}{\partial R}V\right\rangle$ =	610 $km\text{-}sec^{-1}AU^{-1}$	-606 $km\text{-}sec^{-1}AU^{-1}$
$\left\langle \frac{NR^2}{1\ AU^2}\right\rangle$ =	10 cm^{-3}	10 cm^{-3}
$\left\langle \frac{\partial^2}{\partial R^2}V\right\rangle$ =	2.6×10^{3} $km\text{-}ssec^{-1}AU^{-2}$	-2.6×10^{3} $km\text{-}sec^{-1}AU^{-2}$
$\frac{X}{1\ AU^2}$ =	5.4×10^{-16} $cm^{-4}sec^{-1}$	3.2×10^{-16} $cm^{-4}sec^{-1}$

TABLE 4- Energy Balance for Three Shocks

Time	1979 13 1507		1979 17 2056		1979 176 1920	
	upstream	downstream	upstream	downstream	upstream	downstream
N_p	0.073	0.250	0.150	0.240	0.715	1.500
N_c	0.058±.012	0.250±.020	0.150±.010	0.250±.020	1.600±.100	0.970±.010
N_h	0.018±.004	0.023±.004	0.015±.003	0.020±.007	0.010±.003	0.008±.001
$T_i(10^4)$	0.67	7.4	2.2	4.1	3.5	5.0
$T_c(10^4)$	1.7±0.2	6.8±0.2	3.1±0.2	4.0±0.4	3.3±0.1	3.5±0.2
$T_h(10^4)$	32±1	55±20	26±5	43±3	63±13	58±17
U_{1n}	152	49	56	33.6	38	18
B_{1t}	0.71	1.66	0.34	0.60	0.58	0.89
$p_i \times 10^{13}$	0.67±.07	2.6±.03	0.46±.03	1.4±.10	3.5±.70	10.4±.30
$p_c \times 10^{13}$	1.4±.30	2.3±.10	0.64±.04	1.4±.10	4.4±.10	7.7±.50
$p_h \times 10^{13}$	0.8±.20	1.8±.80	0.54±.18	1.2±.30	0.69±.15	0.80±.20
r_1	9.8±.90		4.8±.50		0.80±.20	
$1/\beta_1$	0.7±.07		0.28±.02		0.16	
$(\frac{p_2}{p_1})_{meas}$	2.3±1.0		2.4±0.2		2.2±0.4	
$(\frac{p_2}{p_1})_{pred}$	4.8±0.4		2.3±0.2		1.9±0.2	

TABLE 5. Shock Frequencies, Speeds, and Heating Rates

	Forward Shocks		Reverse Shocks		
	4 AU	8 AU	4 AU	8 AU	
$\langle \nu \rangle$ =	1.16×10^{-6}	0.58×10^{-6}	0.69×10^{-6}	0.23×10^{-6}	sec^{-1}
$\langle U_1 \rangle$ =	160	80	120	50	$km\ sec^{-1}$
$\langle V_S \rangle$ =	570	490	290	360	$km\ sec^{-1}$
$\langle \Delta e (\frac{R}{1\ AU})^2 \rangle$ =	1.2×10^{-10}	4.2×10^{-9}	6.2×10^{-9}	2.0×10^{-9}	$erg\text{-}cm^{-3}$
$\langle h_s (\frac{R}{1\ AU})^2 \rangle$ =	3.9×10^{-17}	4.0×10^{-18}	1.77×10^{-17}	6.5×10^{-19}	$erg\text{-}cm^{-3}sec^{-1}$

TABLE 6. Quasi-Parallel Shocks

Year	Day	Hour	Angle	(B_2/B_1)
1978	204	2258	150°	1.0
	305	1314	152°	1.5
	338	0122	140°	0.9
1979	56	0508	168°	1.1
	260	2329[a]	163°	1.1
	266	0308	150°	0.9
1980	261	2010	60°	1.0

[a]The time of his event is listed in Table 1 as 1979 260-261.

TABLE 7. Slow Shocks

Year	Day	Hour
1979	21	1334
	29	1846
	92	1139
	93	0716
	197	1850
	334	0645
	346	0403
	346	1800
1980	32	0616
	122	1118
	146	0439

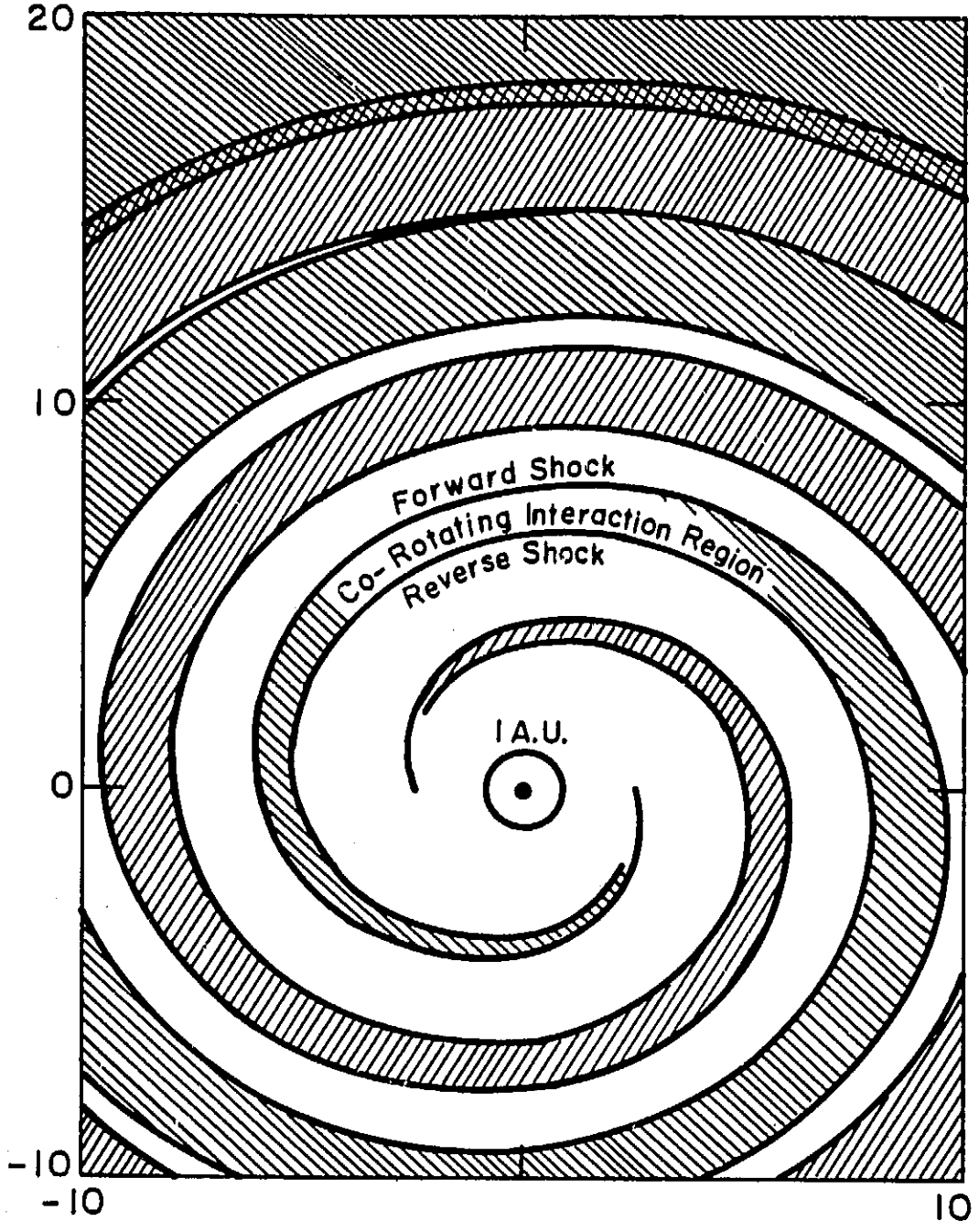

Schematic Representation of Co-Rotating Interaction Regions

Figure 1

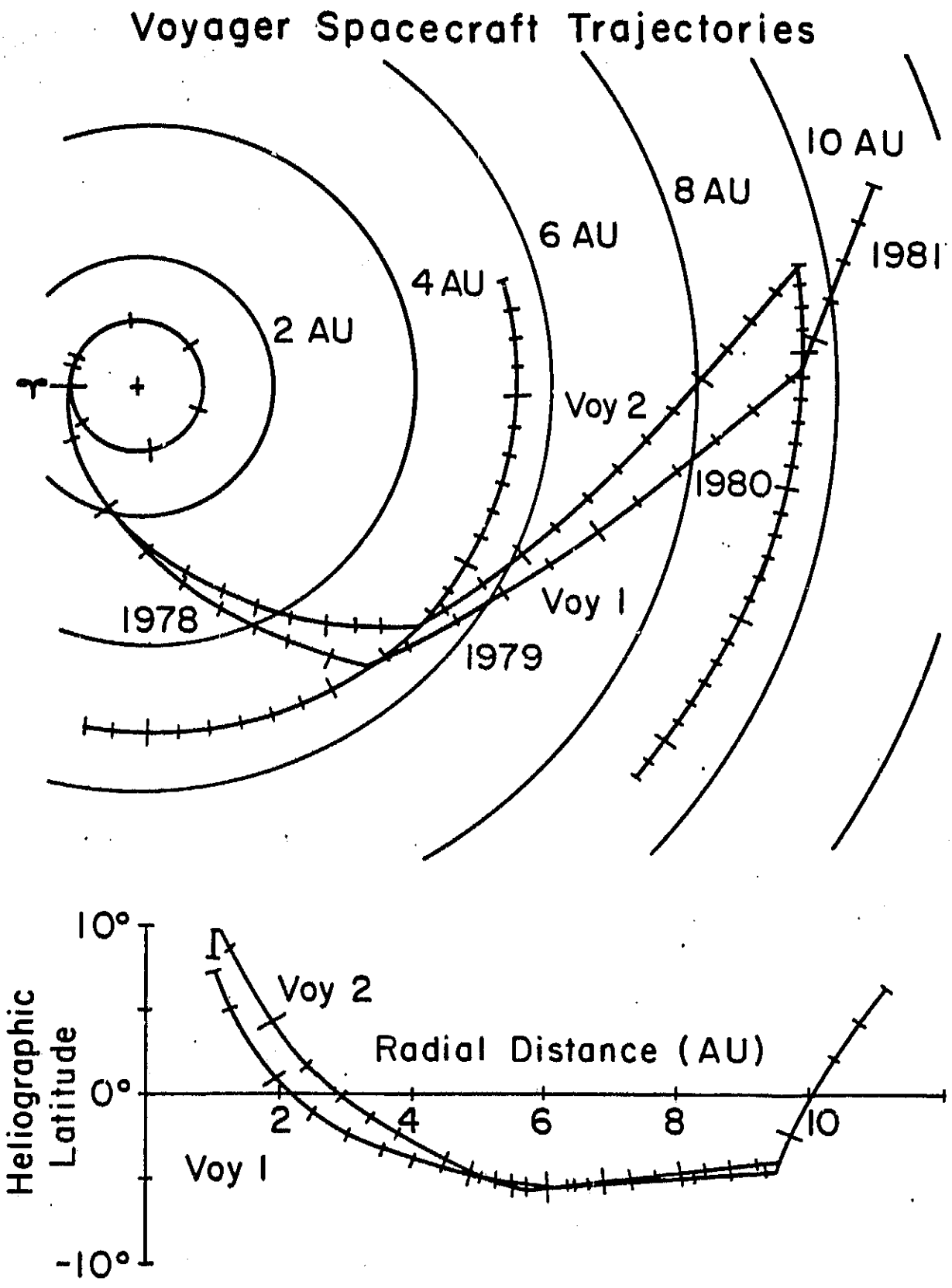
Voyager Spacecraft Trajectories
2 AU
4 AU
6 AU
8 AU
10 AU
1978
1979
1980
1981
Voy 1
Voy 2
10°
0°
-10°
Heliographic Latitude
Radial Distance (AU)
2
4
6
8
10
Voy 2
Voy 1

Figure 2

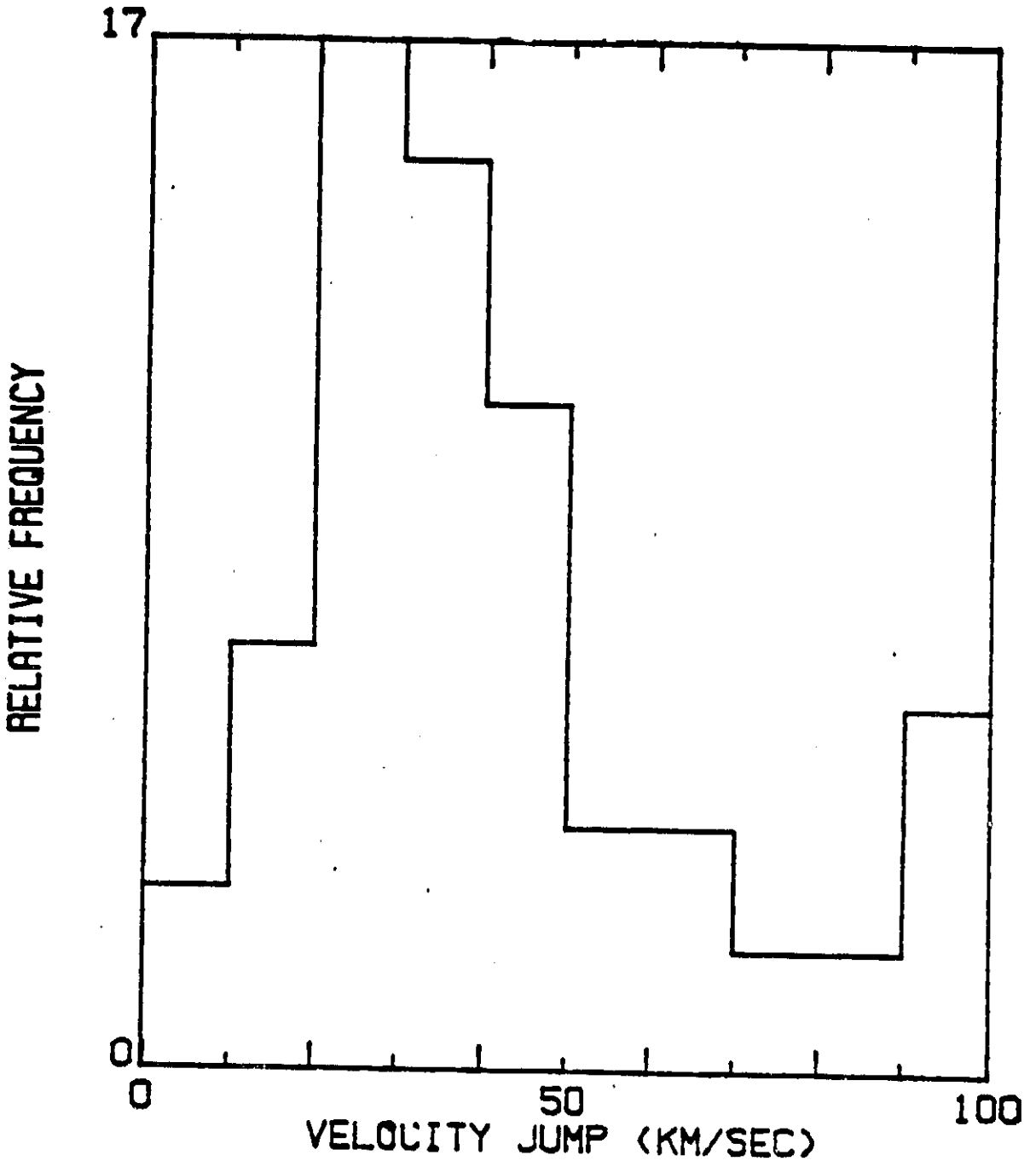
17
0
RELATIVE FREQUENCY
0
50
100
VELOCITY JUMP (KM/SEC)

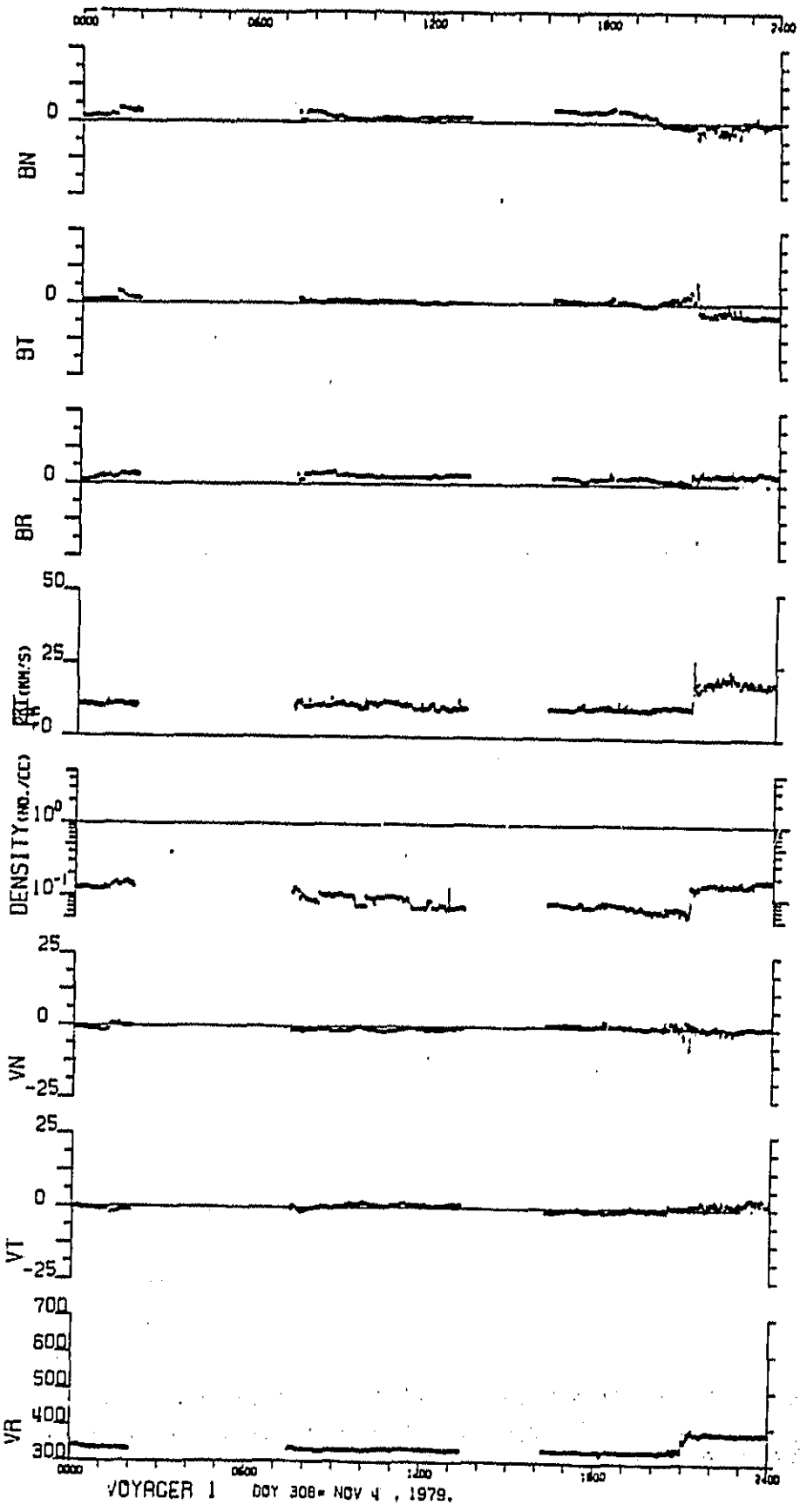

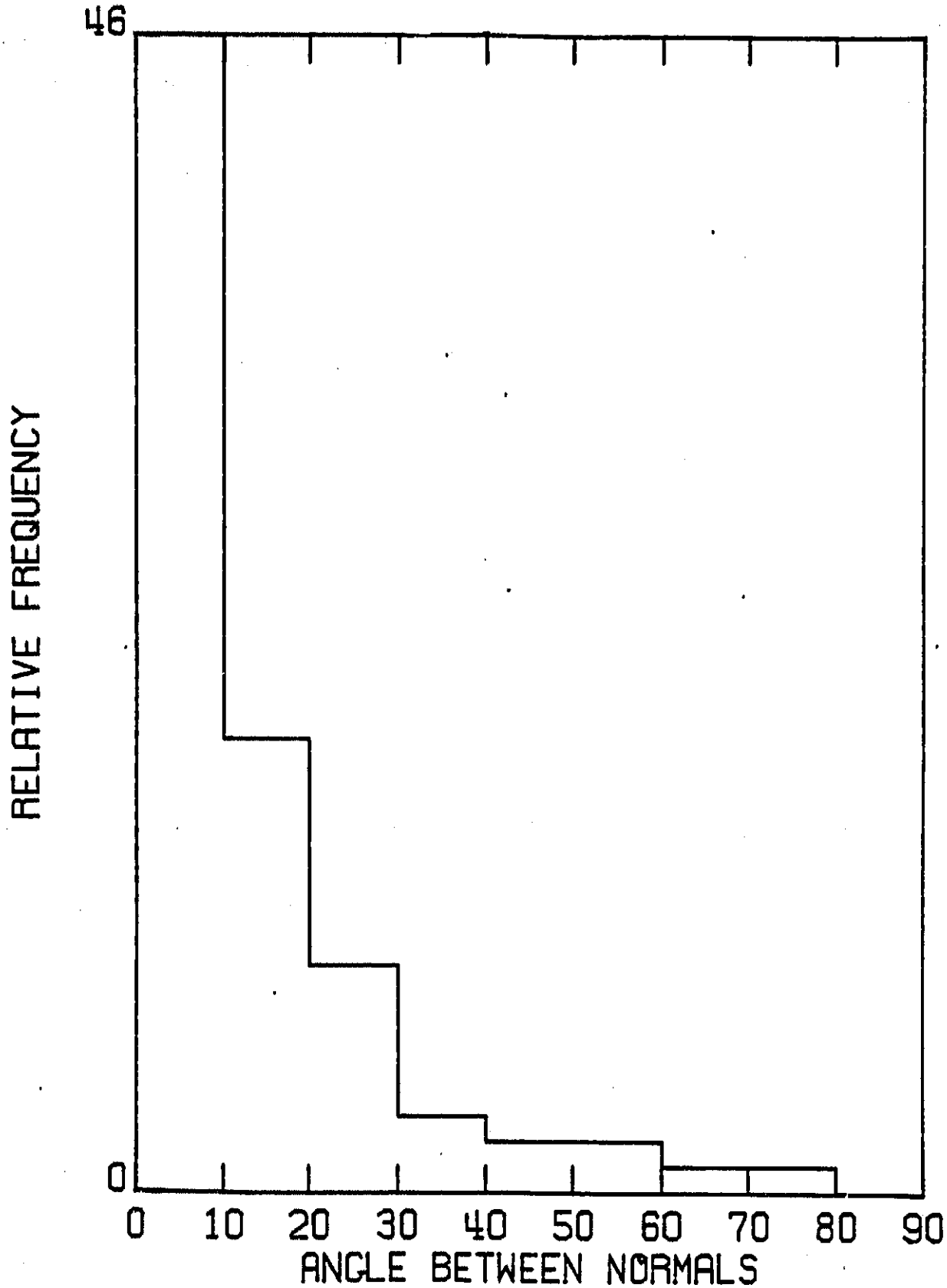
46
0
RELATIVE FREQUENCY
0
10
20
30
40
50
60
70
80
90
ANGLE BETWEEN NORMALS

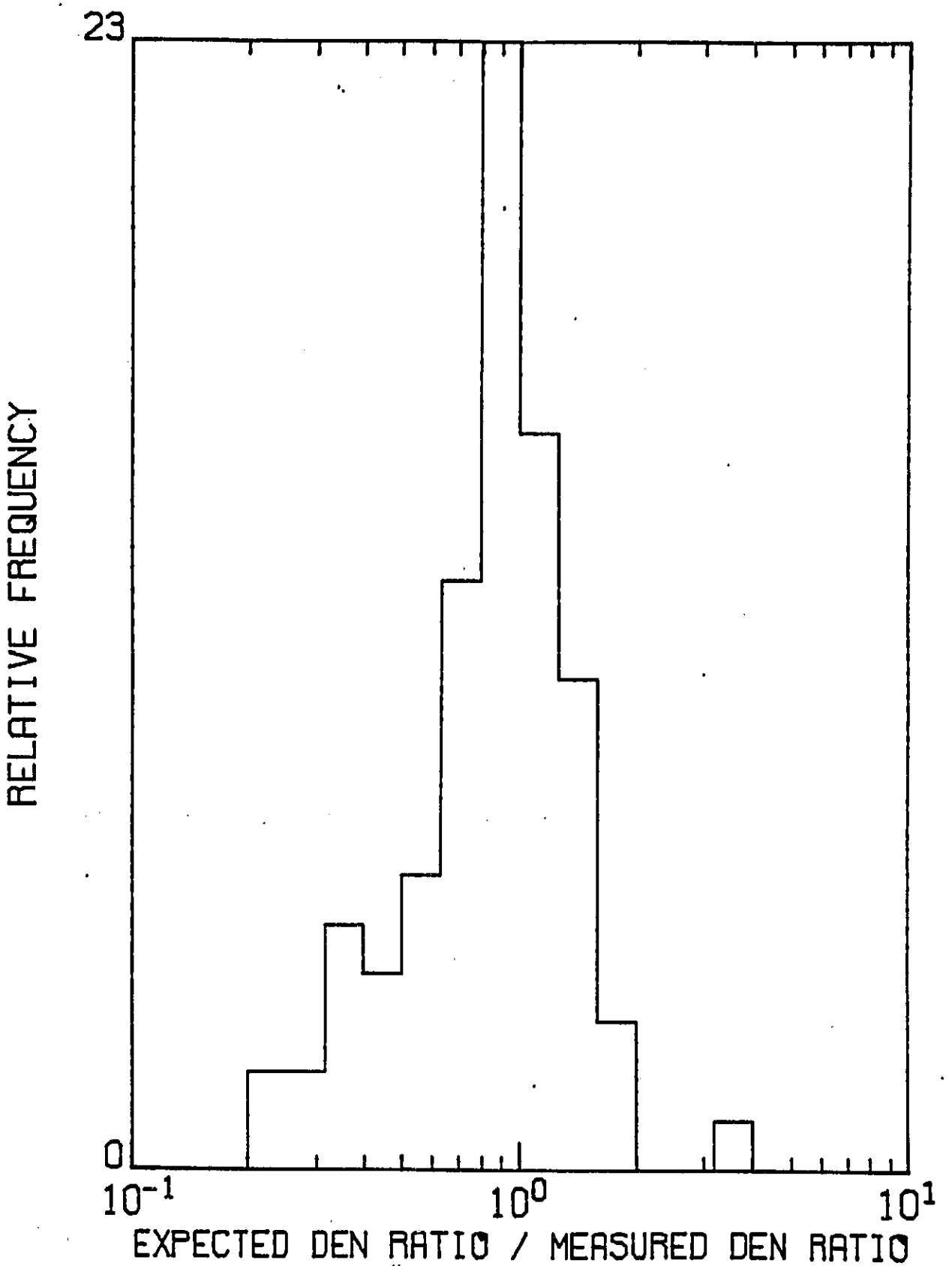
23
RELATIVE FREQUENCY
0
10^{-1}
10^{0}
10^{1}
EXPECTED DEN RATIO / MEASURED DEN RATIO

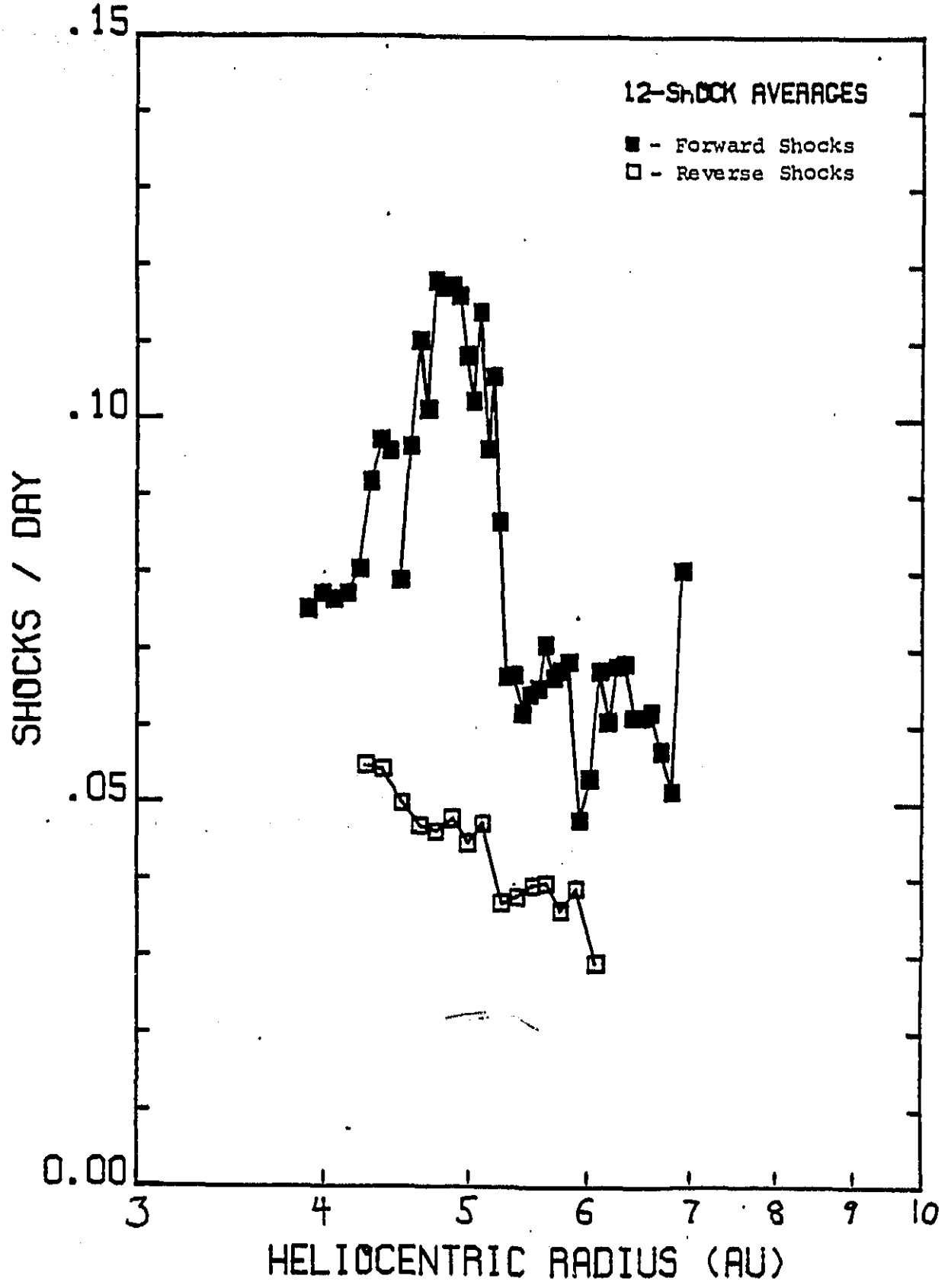

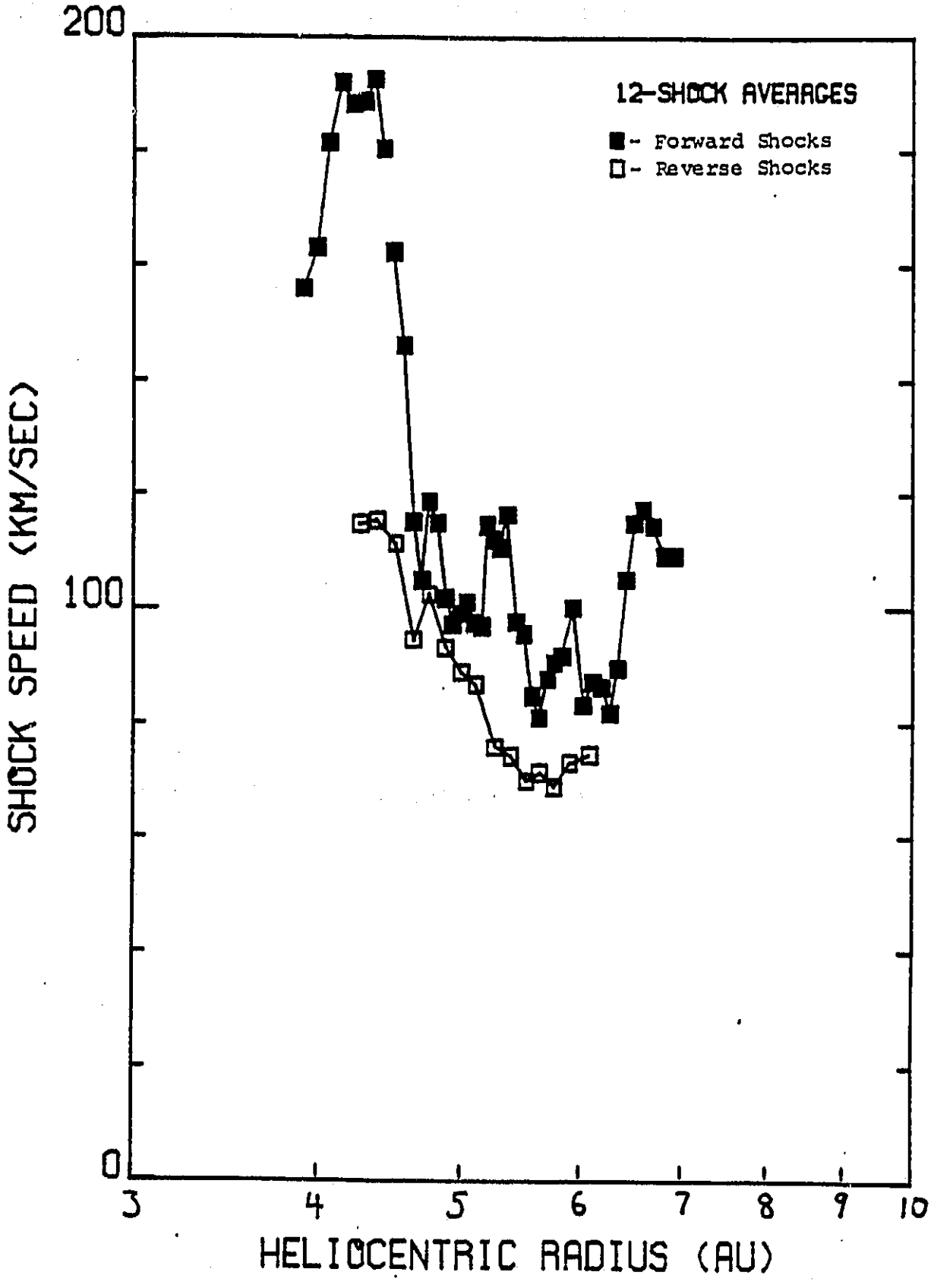

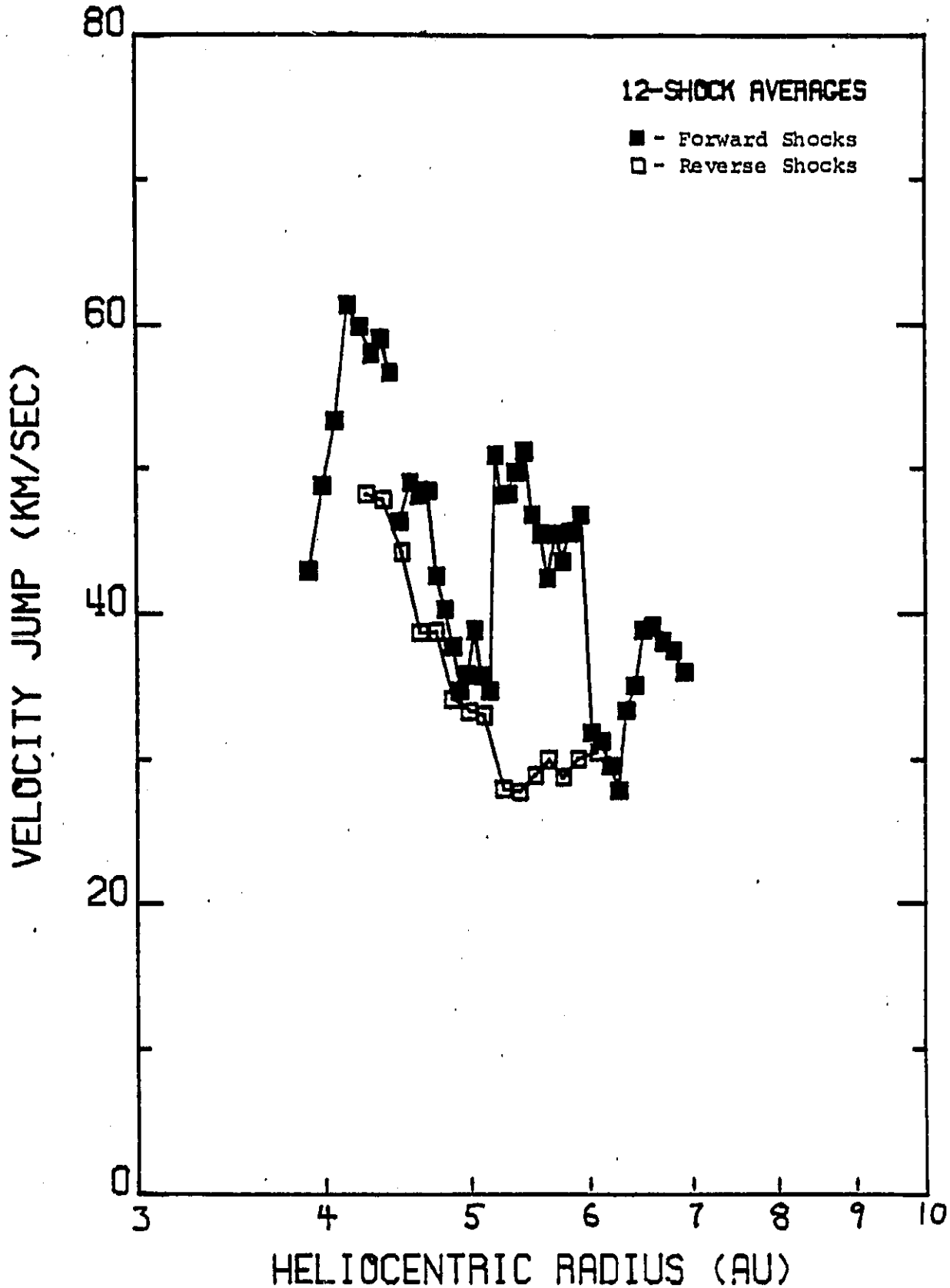
12-SHOCK AVERAGES
■ - Forward Shocks
□ - Reverse Shocks
VELOCITY JUMP (KM/SEC)
80
60
40
20
0
3
4
5
6
7
8
9
10
HELIOCENTRIC RADIUS (AU)

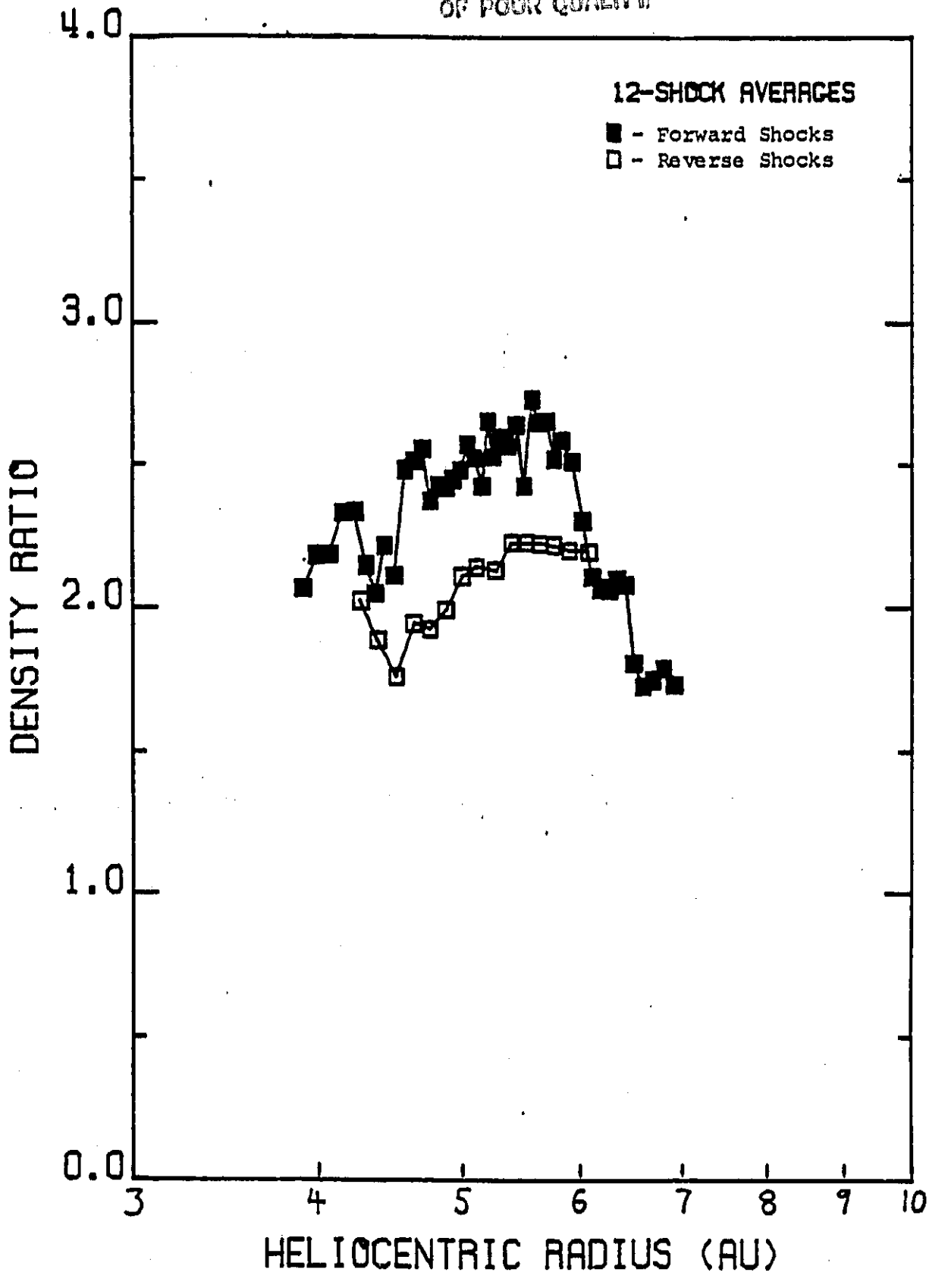

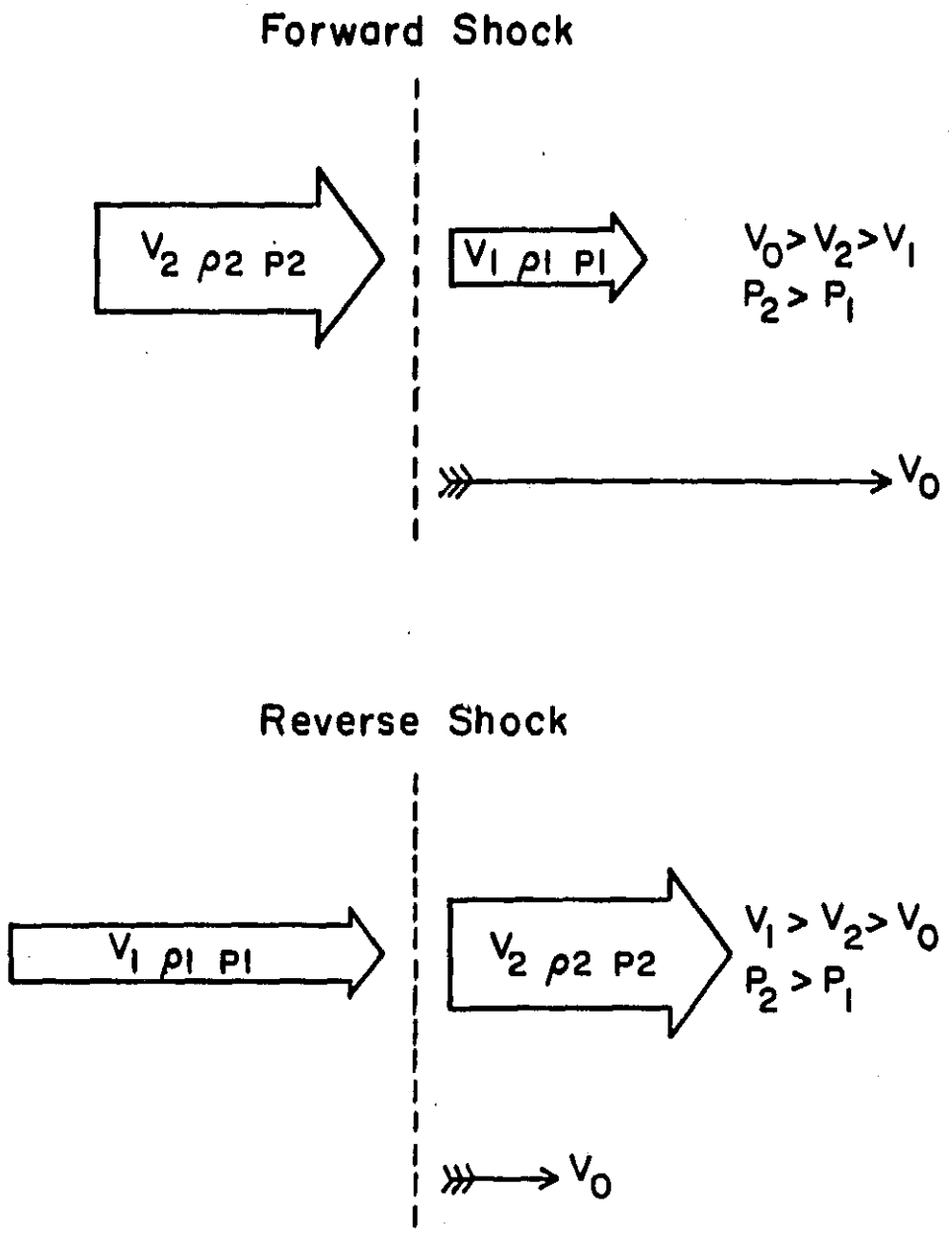
Forward Shock
V2 ρ2 P2
V1 ρ1 P1
V0 > V2 > V1
P2 > P1
V0
Reverse Shock
V1 ρ1 P1
V2 ρ2 P2
V1 > V2 > V0
P2 > P1
V0

Figure 11

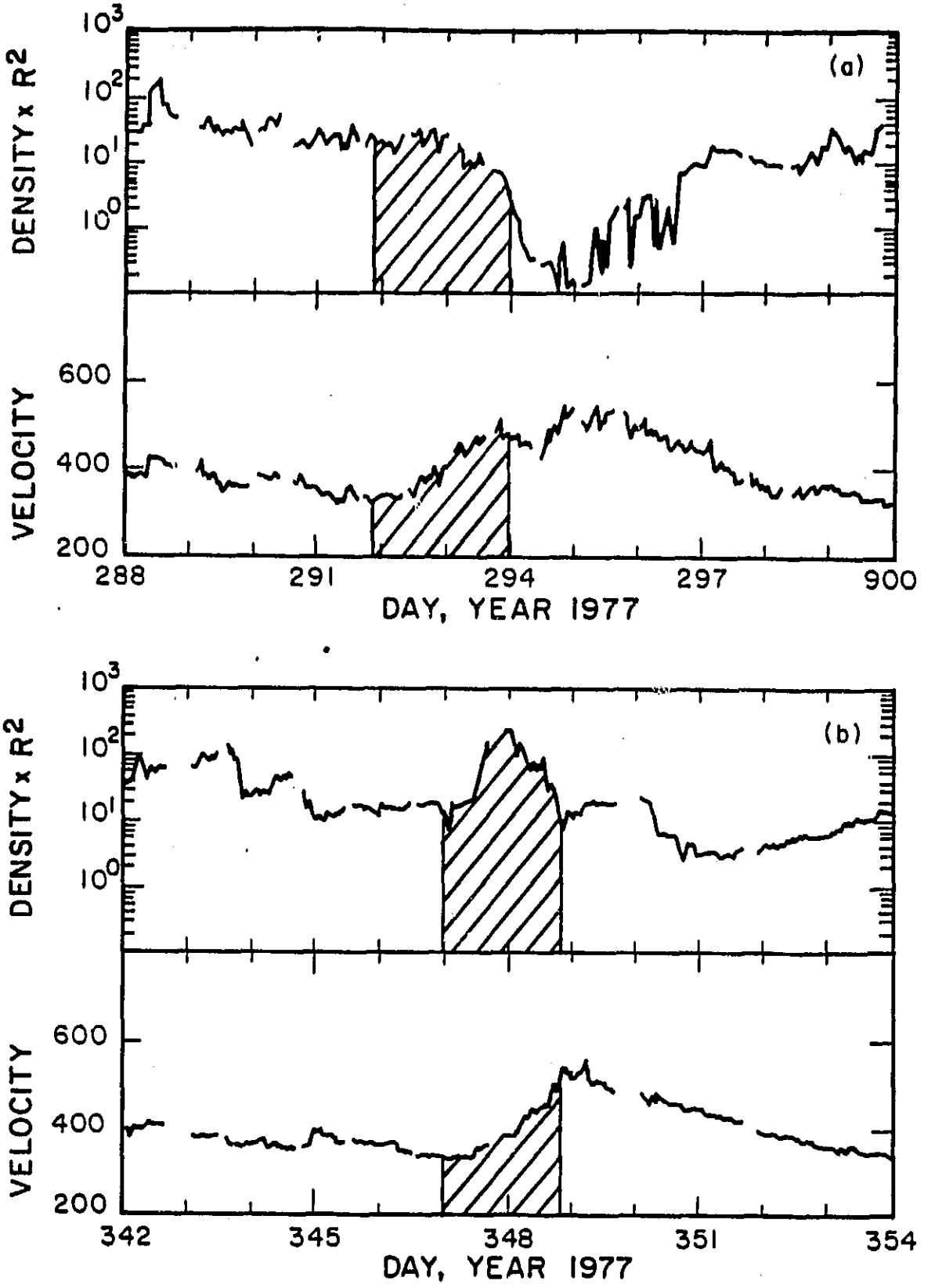

Figure 12

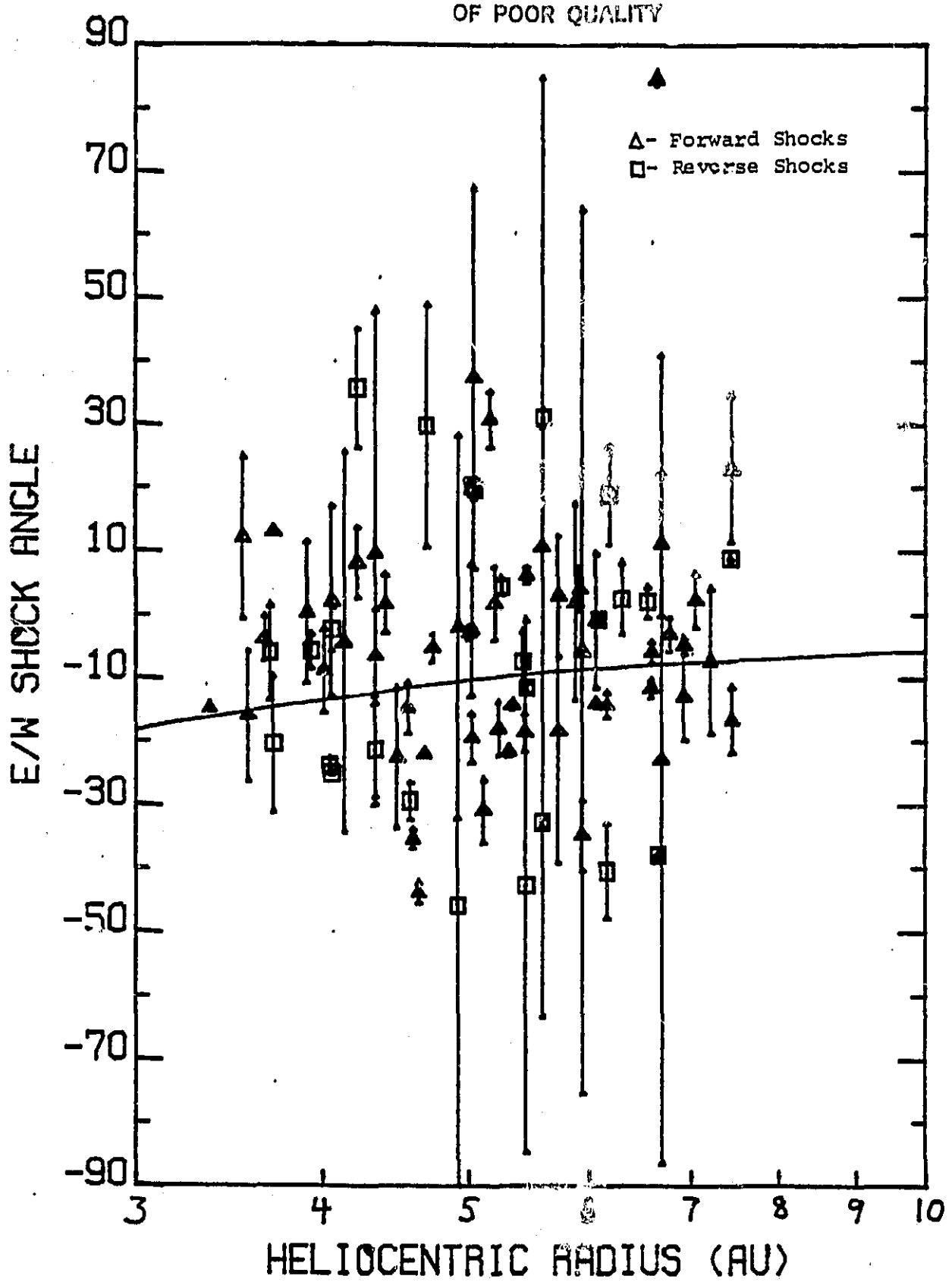

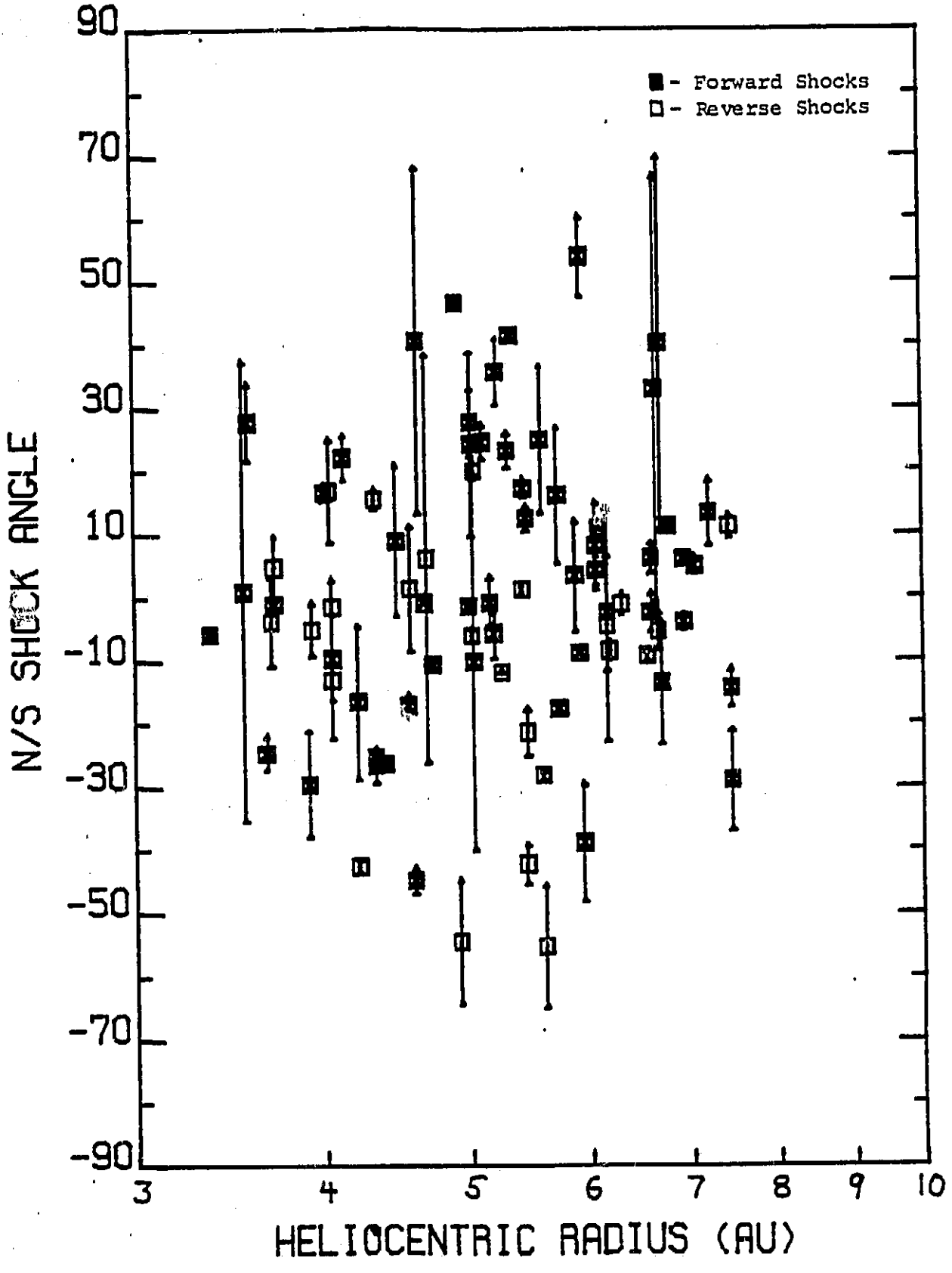

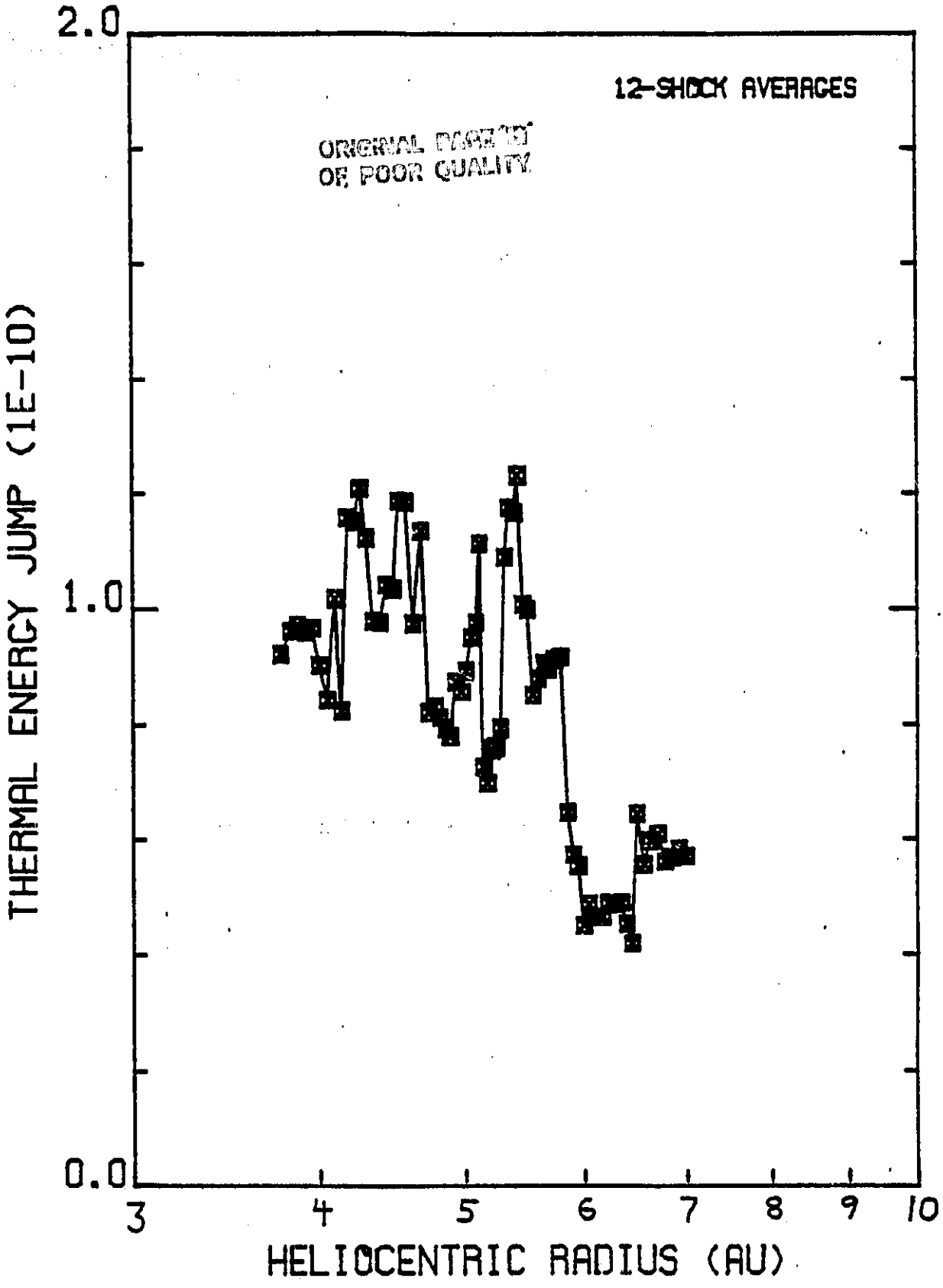
12-SHOCK AVERAGES
ORIGINAL PAGE IS
OF POOR QUALITY
THERMAL ENERGY JUMP (1E-10)
2.0
1.0
0.0
3
4
5
6
7
8
9
10
HELIOCENTRIC RADIUS (AU)